SPACE SCIENCES LABORATORY

FINAL REPORT

NASA Grant NGR 05-003-431

Data Processing of Martian Topographic Information Obtained from Ground-Based Radar & Spectroscopy & from Mariners 6 & 7

Martian Topography Elevations:

Data Processing

2/1/71 - 7/31/72

Principal Investigator: K.A. Anderson

Project Director: R. A. Wells

March 14, 1974

Series 15, Issue 14

UNIVERSITY OF CALIFORNIA, BERKELEY

Space Sciences Laboratory
University of California
Berkeley, Calif. 94720

FINAL REPORT

NASA Grant NGR 05-003-431

Data Processing of Martian Topographic Information Obtained from Ground-Based Radar & Spectroscopy & from Mariners 6 and 7

Martian Topography Elevations: Data Processing

(2/1/71 - 7/31/72)

Principal Investigator

Professor Kinsey A. Anderson

Project Director

Dr. R. A. Wells

March 14, 1974

Series 15 Issue 14

Martian Topography Elevations: Data Processing

Final Technical Report NASA Grant NGR 05-003-431

NASA Grant NGR 05-003-431 was awarded to the Space Sciences Laboratory, University of California, Berkeley on the basis of proposal UCBSSL No. 385 (Revised). The Principal Investigator was Professor K. A. Anderson, Laboratory Director; and the Project Director was Dr. R. A. Wells.

The funds were administered for the purposes of i) preparing a topographical elevation contour map of Mars from all data sources available through 1969, including ground-based radar and spectroscopic CO_2 pressure measurements and the Mariners 6 and 7 pressure observations; and ii) of partially financing an expedition to Cerro Tololo Observatory, La Serena, Chile to observe Mars by spectroscopic methods in 1971 to provide additional pressure data for topographic information.

This report presents the final results and is comprised of the published papers that appeared in the scientific literature as a result of funding from NGR 05-003-431. Funds were dispersed before the project could be completed, and a renewal proposal to continue the project was not re-funded; however, marginal support was made available to the Project Director through the Space Sciences Laboratory general operating funds of NASA for its continuation. This latter funding has resulted in the preparation of a textbook, Morphology of the Planet Mars by R. A. Wells, which incorporates all of the topographic information funded by NGR 05-003-431 as well as additional Earth-based data and the Mariner 9 observations obtained in 1971-72. This text is currently in preparation at D. Reidel Publishing Company, Dordrecht, Holland with scheduled release date approximately in the Summer of 1974. Although the work contains more than just the topographic material referred to above, it can be considered an additional summary for grant NGR 05-003-431.

Following is a list of conference papers and lectures given by the Project Director during the operation of NGR 05-003-431. Following that is a list of the published papers based on NGR 05-003-431 funding. The last item in that list regards the Cerro Tololo results in (ii) of the preceeding page, but was not co-authored by the Project Director— a credit line at the end of that paper acknowledges the Project Director's contributions to the experiment. Since the Project Director did not participate in the preparation of the Cerro Tololo paper, it is accordingly not included with the papers given in this report— a discussion of the results of this experiment can be found in Morphology of the Planet Mars.

Lectures & Conference Papers given by R. A. Wells (NGR 05-003-431; not included here)

1) "Topography of Mars", Geolog. Soc. Amer., NASA sponsored Mars Symposium, Washington, D. C., Nov. 1-3 (1971).

2) "Martian Topography: Final Contour Map from all Data Sources Through 1969", Amer. Astron. Soc., Div. Planetary Sci. Conference, Kona, Hawaii, March 20-24 (1972); appears as an (abstract) by the same title in: Bull. Amer. Astron. Soc., 4, 372 (1972).

3) "Martian, Lunar, & Terrestrial Crusts: A Three-Dimensional Exercise in Comparative Geophysics", Amer. Astron. Soc., Div. Planetary Sci. Conference, Kona, Hawaii, March 20-24 (1972); appears as an (abstract) by the same title in: Bull. Amer. Astron. Soc., 4, 374 (1972).

4) "Martian, Lunar, and Terrestrial Crusts: A 3-Dimensional Exercise in Comparative Geophysics", NATO Advanced Studies Institute, Univ. Newcastle-upon-Tyne, England, April 10-19 (1972); for published report see (5) in following list.

5) "Results from Mariner 9 and Martian Topography", special seminar, *Physique du Système Solaire*, Section d'Astrophysique, Observatoire de Paris, Meudon, France, April 25 (1972).

Published Papers by R. A. Wells (NGR 05-003-431; included in this report):

1) "Analysis of Large-Scale Martian Topography Variations— I: Data Preparation from Earth-Based Radar, Earth-Based CO_2 Spectroscopy, and Mariners 6 and 7 CO_2 Spectroscopy", Geophys. J. Roy. Astron. Soc., 27, 101 (1972).

2) "Relief-Darstellung der Marsoberfläche", (in German), Umschau, 72, 293 (1972).

3) "ТОПОГРАФИЯ МАРСА ПО ДАННЫМ НАЗЕМНЫХ РАДИОЛОКАЦИОННЫХ ИЗМЕРЕНИЙ И ПО НАБЛЮДАЕМОМУ С ЗЕМЛИ И С КОСМИЧЕСКИХ АППАРАТОВ 'МАРИНЕР-6 И 7' ПОГЛОЩЕНИЮ CO_2", (in Russian), Astron. Zhur., 49, 607 (1972).

4) "Mars: Are Observed White Clouds Composed of Water?", Nature, 238, 324 (1972).

5) "Martian, Lunar, and Terrestrial Crusts: A 3-Dimensional Exercise in Comparative Geophysics", in Implications of Continental Drift to the Earth Sciences, vol. 2, ed. by D. H. Tarling and S. K. Runcorn, 1099, Academic Press, London (1973).

A detailed discussion of Earth-based and Mariner spacecraft observations of Mars can be found in (preliminary announcement only, included here):

6) Morphology of the Planet Mars, R. A. Wells, D. Reidel Publ. Co., Dordrecht, Holland, in preparation (1974).

The results of the Cerro Tololo CO_2 mapping experiment was issued as (not included here):

7) T. D. Parkinson and D. M. Hunten, "CO_2 Distribution on Mars", Icarus, 18, 29 (1973).

Geophys. J. R. astr. Soc. (1972) **27**, 101–133.

Analysis of Large-Scale Martian Topography Variations—II

Data Preparation from Earth-Based Radar, Earth-Based CO_2 Spectroscopy, and Mariners 6 and 7 CO_2 Spectroscopy

R. A. Wells

(Received 1971 July 23)

Summary

Four series of investigations have produced data on Martian topographical variations at spatial resolutions ranging from about 100 to 1000 km. These experiments were based on the two independent techniques: direct radar ranging of surface heights on Mars and spectrophotometric observations of absorptions produced by CO_2 molecules in the Martian atmosphere.

Primary problems associated with the preparation of a systematic distribution of surface heights from the four data sets involve the determination of a zero altitude level common to all sources and the reorganization of the data points onto a regular grid network. The results of this data combination process are the production of a surface height contour map and the preparation of a table of surface heights spaced on a $5° \times 5°$ grid interval. Only the contour map and difficulties associated with the data preparation are presented with this article; the 5°-grid data form a part of a more detailed analysis of Martian height variations which will follow in a second paper.

Briefly, Mars possesses unexpectedly pronounced topography which can have important geophysical consequences. The contour map of Mars clearly reveals a structural complex of blocks and basins whose distribution enhances the magnitude of low-degree surface harmonics.

1. Introduction

The planet Mars has long been the target of many kinds of astronomical observations. Of all the bodies in the solar system, Mars possesses unique observational characteristics. Its periodic close approaches to the Earth permit relatively high-resolution ground-based studies to be made: its atmosphere, sufficiently dense for spectroscopic observations, is nevertheless thin and clear enough to enable features on the surface to be seen. As a relatively large member of the 'terrestrial' group of planets with two moons, it also presents the possibility of having responded to highly interesting geodynamical processes.

A comprehensive knowledge of the topographical relief at all scales on Mars is fundamental in the continued observational and theoretical exploration of the planet. Such information on large scales bears not only on the shape of the surface itself, but also on the relationships with stress/strain effects in the outer crustal layers, the state of the interior of the planet, and influences on dynamical motions in the

atmosphere. Smaller-scaled relief provides data on environmental processes such as regional structuring, localized weather effects, and mass transport of various atmospheric constituents near ground level. All of these phenomena can affect the choices of landing sites for future spacecraft missions. Many facets of scientific interest would thus be served by a more precise morphological definition of the Martian surface.

Large-scale relief measurements, with which this report is concerned, have been derived from two theoretically independent techniques. One is radar ranging, in which surface heights at the Martian sub-Earth points are directly related to delays in returning radar echos; and the other, high-resolution CO_2 spectroscopy, in which the abundance of CO_2 in vertical columns above spatially limited areas is deduced from absorptions in particular CO_2 bands. The abundance determination provides a value for the surface pressure of CO_2 which can be converted to a surface altitude above some zero upon adoption of a particular atmospheric model.

Since 1967 these two techniques have been utilized by four diverse groups of investigators. These sources are: (1) the 1967 radar measurements by Pettengill *et al.* (1969), and the 1969 radar determinations by Rogers *et al.* (1970) using the Haystack facility; (2) the 1969 radar measurements by Goldstein *et al.* (1970) using the JPL Goldstone antenna; (3) the ground-based CO_2 measurements made at the Kitt Peak National Observatory by Belton & Hunten (1969, 1971) and Wells (1969a); and (4) the Mariner 6 and 7 CO_2 observations of Herr *et al.* (1970). In addition, data from the UV experiment on Mariners 6 and 7 were utilized to deduce surface heights from pressures calculated from UV albedos (Barth & Hord 1971). However, since this method can be strongly influenced by localized brightness variations caused by fluctuating aerosol distributions in the atmosphere, no attempts were made to include these data in this analysis. (Since this report went to press these data have been finalized and will be included in Paper II.)

This paper presents a combination of the above data sources into a homogeneous system of surface heights. Each source is treated under the separate headings 2–5; the preparation of the combined regular array of data is given in Section 6; and some discussion of results are given in the final Section 7. A more detailed accounting of results is deferred to Part II of this paper which will separately treat a harmonic analysis on the data discussed here.

2. The 1967 and 1969 Haystack Radar Data

The most extensive radar observations of Mars are those of Pettengill *et al.* (1969) and Rogers *et al.* (1970). The altitude determinations are limited to the Martian sub-Earth points which varied from approximately 0° to about 22° N latitude during the course of observations over two apparitions (1967 and 1969) of Mars. The distribution of points is shown on a Mercator projection representing the surface of Mars with co-ordinates in the astronomical sense of South at the top and longitude increasing from 0° to 360° towards the West, Fig. 1. The data table used in this paper is that found in the special report issued by the Lincoln Laboratory (Rogers *et al.*, 1970). This table combines both the 1967 and 1969 observations; however, for the 1967 data the latitude of each point is listed at a constant 22° N. To find the actual variation, reference was made to Pettengill *et al.* (1969) for observation times from which the Martian sub-Earth points could be calculated.

Instrumental and geometrical parameters defined the spatial resolution of the series of observations to be a circle on the surface of Mars of about 300 km diameter centred at each point. In the smoothing procedure which placed the uneven distribution of data shown in Fig. 1 onto a regular grid, this resolution limit was increased to about 1000 km (as was each of the subsequent data sources) to match that of the ground-based CO_2 measurements, the lowest resolution of all the data groups.

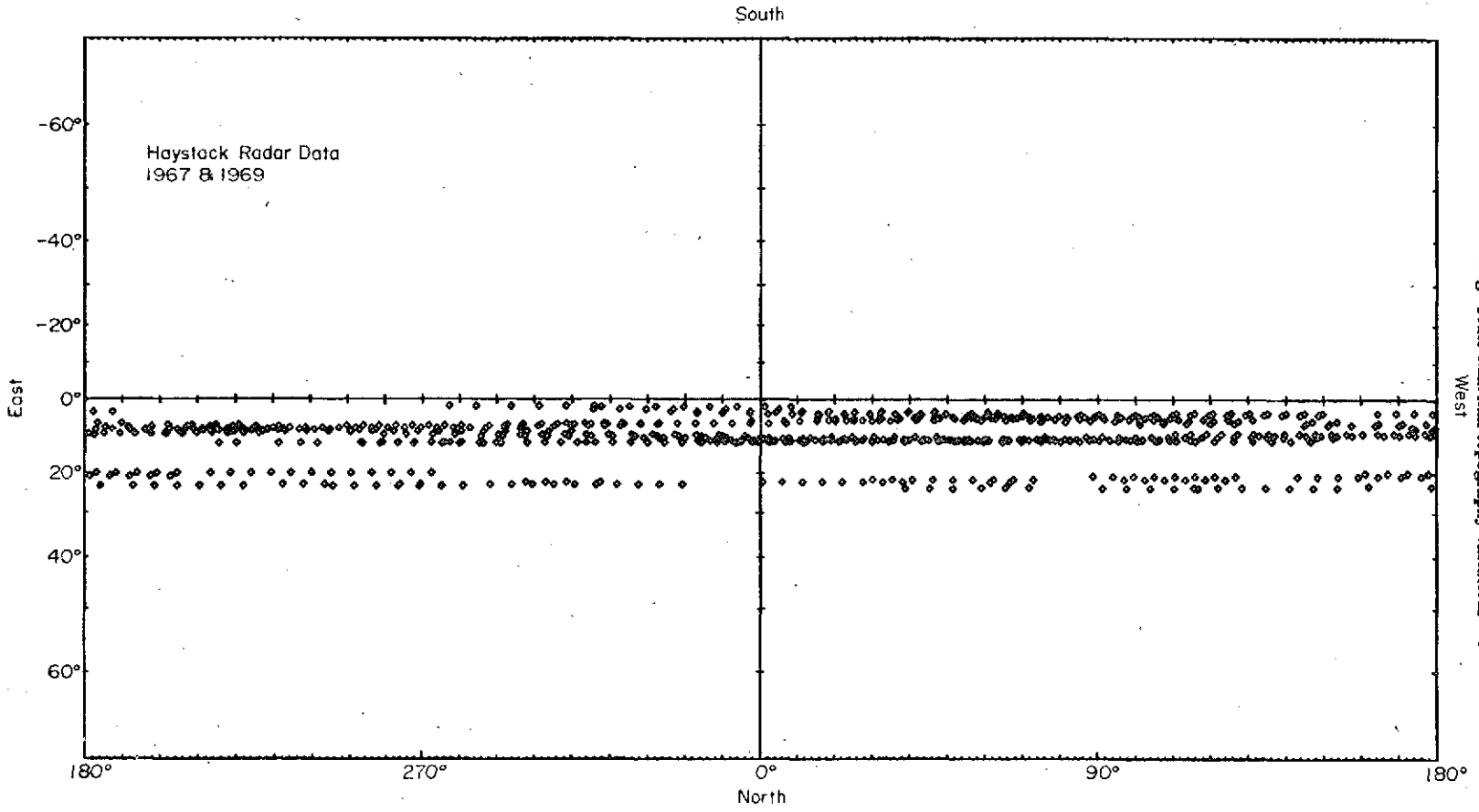

FIG. 1. The distribution of 700 radar measurements combining those of Pettengill *et al.* (1969) with those of Rogers *et al.* (1970) made with with the Haystack antenna at the 1967 and 1969 apparitions of Mars. South is at the top and longitude increases to the West. Refer to the map in Fig. 20 to see the location of these points with respect to the dark and bright area on Mars.

The basic smoothing equation is simply:

$$\bar{Z} = \frac{\sum_i^n \{z_i \exp[-(r_i^2/2\sigma^2)]\, w_i\}}{\sum_i^n \{\exp[-(r_i^2/2\sigma^2)]\, w_i\}}, \tag{1}$$

where the weighted mean height $\bar{Z}$ is calculated from each height z_i after filtering by a circular Gaussian function and an appropriate weighting function w_i. The two-dimensional Gaussian function was chosen so that at the resolution limit (a circle of 9° radius; 18° ≃ 1000 km) its value equalled $1/e$; hence, $\sigma^2 = 40{\cdot}5\,(\text{deg}^2)$. The distance in degrees, r_i, from the grid interval to each datum within the 9°-radius circle was calculated by spherical trigonometry.

For these particular radar data, the weighting function w_i was calculated from the standard deviations, ρ_i, of the altitudes listed in the tables. A check was made to insure a random distribution of ρ_i, which would avoid preferential weighting, Fig. 2. Since this is the case, then $w_i = \rho_i^{-2}$.

The distribution of data points was such that a 5° × 5° regular grid of values could be calculated from equation (1). Since it was desirable to obtain a measure of the accuracy of the smoothing process, weighted mean standard deviations were calculated for each grid point from

$$\bar{s}^2 = \frac{\sum_i^n \{(\bar{Z}-z_i)^2 \exp[-(r_i^2/2\sigma^2)]\, w_i\}}{(n-1)\sum_i^n \{\exp[-r_i^2/2\sigma^2)]\, w_i\}} \tag{2}$$

At least three data points were constrained to be located within a resolution circle before a $\bar{Z}$ or $\bar{s}$ could be calculated. In general, the resolution circles were well populated except in a few places near the northern or southern extremes of the scans.

The purpose of calculating $\bar{s}$ is twofold. Firstly, the values can be contoured and the relationship of the degree of accuracy in the smoothing operation can be easily followed from area to area. Second, the values of $\bar{s}$ are in consistent units between the four data sets and can therefore be used as weighting factors in the final

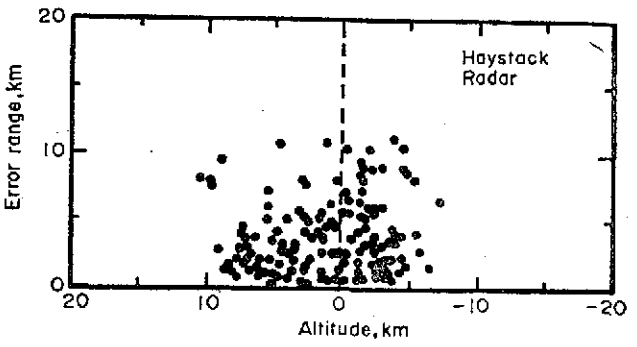

FIG. 2. A plot of the error range (sum of the absolute values of the ± standard deviation of each measurement) against altitude for the Haystack radar data. A large portion of the 700 determinations had error ranges less than 1 km and are left off the bottom edge of the diagram for clarity. The distribution is seen to be random.

combination process described in Section 6. (It will be noticed that the weighting factors for the z_i in each data group are different. Haystack radar: reciprocal variance in km^{-2}; Goldstone radar: reciprocal variance in sec^{-2}; ground-based CO_2 and Mariner CO_2 data: reciprocal natural log of the airmass. The weighting factors for the final combination, however, are reciprocal variances in km^{-2} determined from $\bar{s}$ and are the same type of number between the groups.)

The 700 data points shown in Fig. 1 generated a $5° \times 5°$ grid of 438 values between $-5°$ S and 25° N latitudes. These values were fed into a computer with a contouring program which produced the height contours shown in Fig. 3. The distribution of $\bar{s}$ associated with these values is given in Fig. 4.

The graph in the upper right corner represents the mean of the values of $\bar{s}$ averaged over the latitudes for each longitude and aids in the reading of the contour map below. Wherever a peak occurs in the graph or a concentration of concentric contour lines drawn at regular intervals from 0·1 to 1·5 km in 0·1 km steps. Large errors can arise from poorly populated resolution circles which contain data values of large spread in standard deviations. Thus, Fig. 4 merely indicates areas where more reliable data would have been desirable.

Although the values of $\bar{s}$ only range between 0·04 and 1·45 km (0·13 to 0·72 km in the mean graph), the location of the peaks is of interest. They generally correspond to elevated areas or slopes on Mars (cf. Fig. 3). At this stage in smoothing, this observation might depend on the possibility that fewer data points were obtained when slopes and elevations were in the field of view than when flatter terrain was available for measurement. Fig. 1 does not provide a definitive answer since there are both many measurements of the slopes in Tharsis and also fewer determinations of the eastern slope of Syrtis Major (λ 120° and 280°W, respectively; see also Fig. 10). However, another interpretation of these correlations in Fig. 4 is that slopes would tend to distort the reflected radar signal more than flat areas.

The radar data were originally reduced assuming a spherical planet. In actuality, Mars is an oblate spheroid with flattening somewhere between 0·012 and 0·005 (the optical and dynamical determinations, respectively). Between the equator and the extremes of the radar scans, the oblateness can cause a shift in the zero level of about 2 km relative to the mean spheroid. However, such small changes in the radius of the planet would be very difficult to detect using radar methods. For example, Rogers *et al.* (1970) give their best mean radius determination as 3393 ± 8 km (error limit is three times the formal error, i.e. the standard deviation).

They reduced the 1967 scan by a constant 3 km to provide a common zero level with the 1969 data. This was due to the choice of a single, specific point in 1967 as that series' reference level. The radar zero level now refers to the mean radius of the planet. This zero level is maintained throughout the remainder of this report for reasons which will become apparent.

3. The 1969 Goldstone Radar Data

A second, independently conducted series of radar observations was performed by Goldstein *et al.* (1970) with the Goldstone radar antenna at the Jet Propulsion Laboratory. These observations ranged in extent from approximately 3° to 13° N latitude. The distribution of points is given in Fig. 5.

A zero level check with the Haystack data was provided by comparing a plot of the Goldstone data on an overlay grid. In general, the Goldstone data were well within the error limits of the Haystack data at all longitudes. There was a small difference in the mean values, however: the Goldstone mean was +0·25 km compared with +0·91 km for the Haystack mean. For consistency, the Goldstone data were therefore increased by +0·66 km before smoothing.

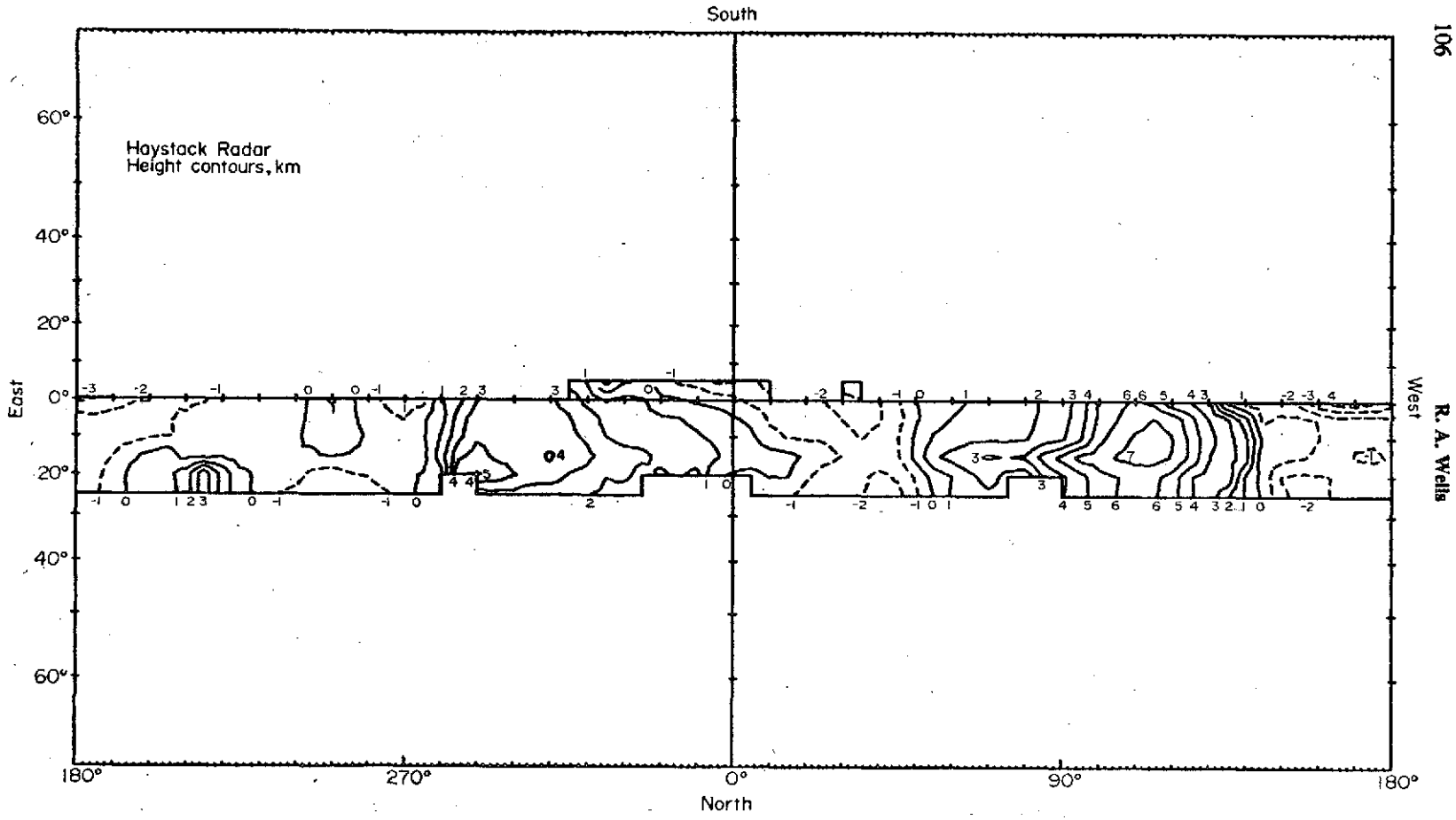

FIG. 3. Altitude contours of the Haystack radar data after smoothing to a 5° grid interval in latitude and longitude and an increase in the spatial resolution from 300 km to 1000 km. The contours were calculated in 1 km steps and drawn by a computer program based on linear interpolation. The contours range from −4 to +7 km. Solid lines represent positive topography (and zero height), and dashed lines represent negative topography.

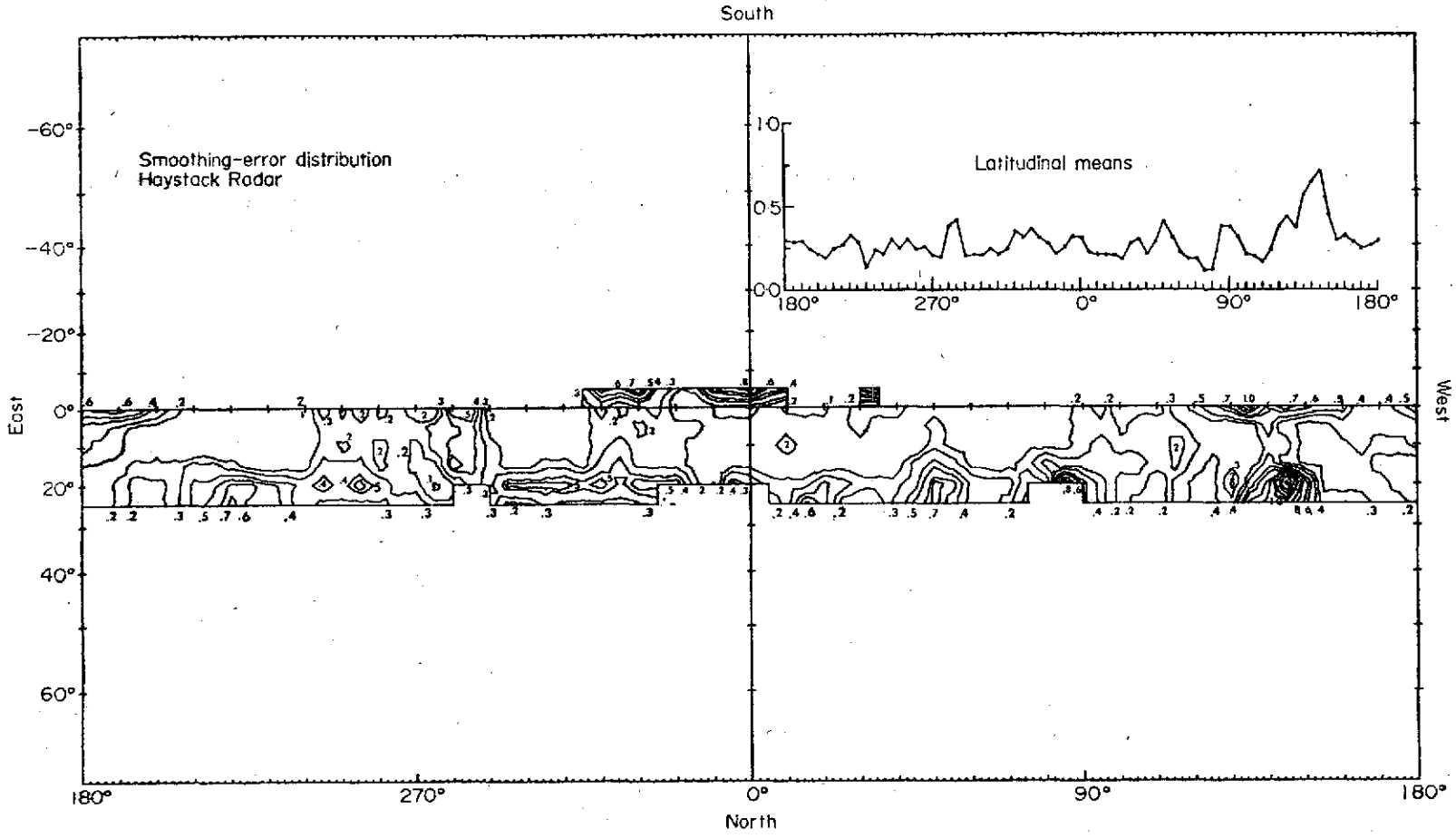

FIG. 4. Contours of the internal errors $\bar{s}$ associated with the smoothing calculations of equation (1) for the Haystack data. The diagram in the upper right corner shows the mean error over latitude as a function of longitude. Compare peaks with concentric contours in the map below. The largest errors are associated with high altitudes or slopes in the topographic map, Fig. 3. The contours are calculated in 0·1 to 1·5 km.

The resolution of these observations was a rectangular element centred at each point extending 220 km in longitude and 90 km in latitude. The difference in the shape of the resolution element compared with the Haystack data is due to differences in range-gating procedures used by the two groups. The smoothing calculation, of course, increases this limit to 1000 km.

The data tables, generously provided to the author by R. M. Goldstein, did not contain error limits (standard deviations) for the microsecond delay (or altitude) measurements. However, errors were listed for the measured-minus-predicted Ephemeris flight times of the echos which are related to altitudes. The reciprocal square of these values were therefore used as the weighting factors w_i in equations (1) and (2).

The remainder of the calculations with these equations were as before. The 236 data points (Fig. 5) generated a 5° regular grid of 250 values between 0° and 15° N latitude. The resulting computer plot of height contours from these values is given in Fig. 6. Associated with these values, corresponding error limits $\bar{s}$ were also calculated, Fig. 7. As before, the upper diagram is the mean of $\bar{s}$ with the two-dimensional distribution given by the contour map below.

It is of interest to compare Fig. 7 with Fig. 4. In the Goldstone case, the internal errors from smoothing only ranged between 0·06 and 1·08 km (contour intervals are 0·1 km ranging from 0·1 to 1·0 km), somewhat better than the Haystack results of the previous section. However, the locations of peaks in the error limits are strikingly close between the two data sets. The suggestion that slopes might disperse the radar signals more than flatter terrain is therefore strengthened.

4. The Kitt Peak spectroscopic CO_2 measurements

The technique of determining surface heights on Mars by ground-based infrared spectroscopy was devised primarily by M. J. S. Belton and D. M. Hunten at the Kitt Peak National Observatory. It was first utilized sucessfully by these investigators and by the author during the 1969 Mars apparition with the McMath solar telescope. Preliminary results were published by Belton & Hunten (1969) and by Wells (1969a). The final, comprehensive report including the theoretical mathematical derivations, as well as the observations of the Kitt Peak group, can be found in Belton & Hunten (1971). The observations conducted by the writer utilizing the same equipment will be detailed in this section.

The instrumental design, derivation of equations leading to Martian surface pressures, and discussions of various limitations of the observing technique will not be repeated in full in this report. This section is limited to a continuation of Belton & Hunten's (1971) Table 4 of measured points and the preparation of the ground-based CO_2 height values for the final combination with other data sources.

If p_{CO_2} is the partial pressure of CO_2 at a specified point on Mars; η, the airmass factor; T, the air temperature; S_1, the number of counts in the data accumulator from the 1·05 μ lines (R-branch); and S_O, the reading in the data channel from a standard source, then according to Belton & Hunten (1971):

$$\eta p_{CO_2} = C f(\eta, p_{CO_2}, T)[\gamma S_O - S_1], \tag{3}$$

where γ and C are calibration constants. S_O is the reading on diffused light from a tungsten lamp, and γS_O corresponds to the reading on the Moon, i.e. the standard of zero absorption (the Moon has no atmosphere) used in this analysis. The function $f(\eta, p_{CO_2}, T)$ is derived from a weighted mean curve-of-growth of CO_2; and the constant C, a function of the efficiency of the instrument, must be derived from the observations on a night-to-night basis, particularly since the instrumental set-up had to be taken down each morning and arranged and recalibrated each night.

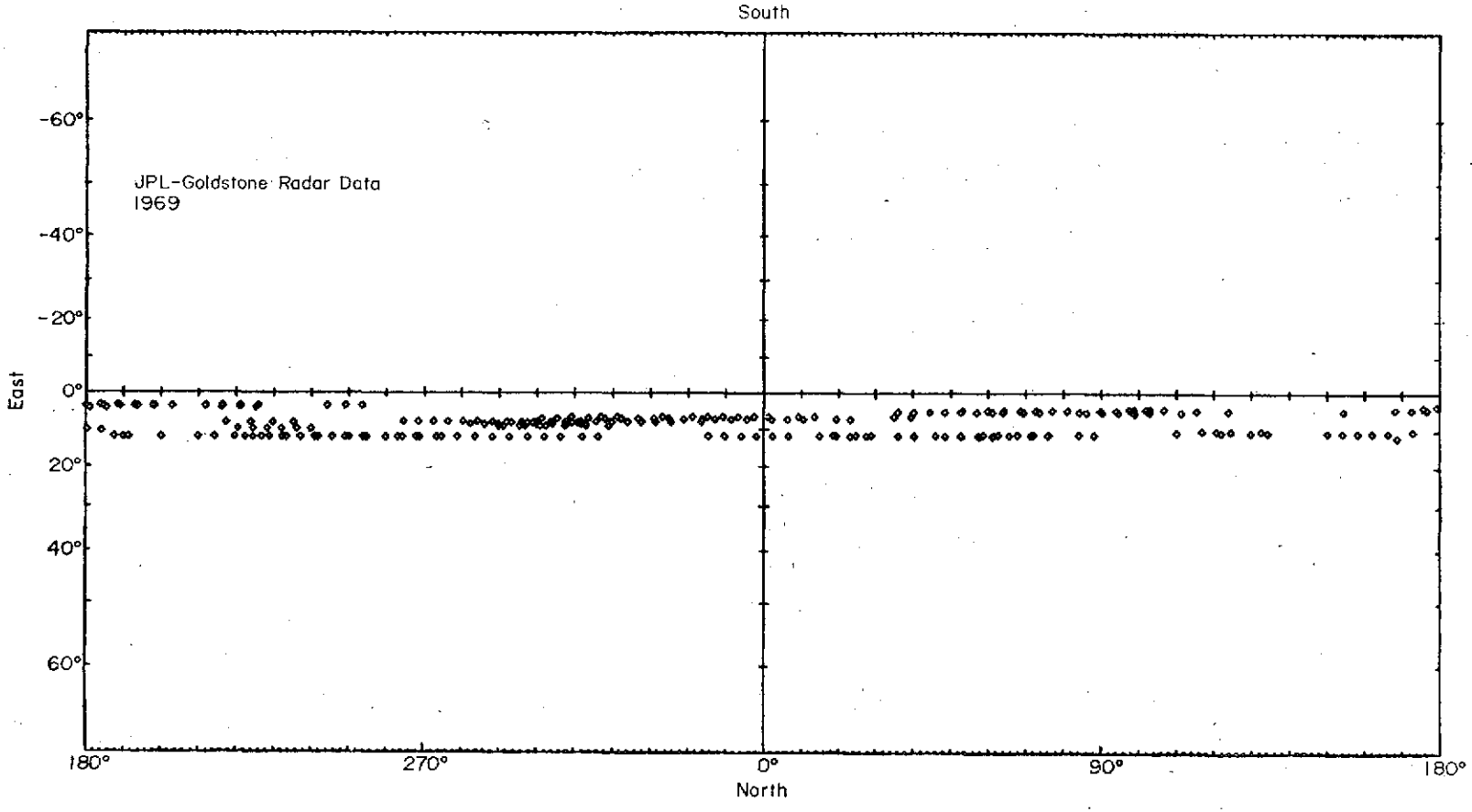

FIG. 5. The distribution of 236 radar measurements made by Goldstein *et al.* (1970) with the JPL Goldstone antenna during the 1969 Mars apparition. Refer to Fig. 20 for their location on Mars.

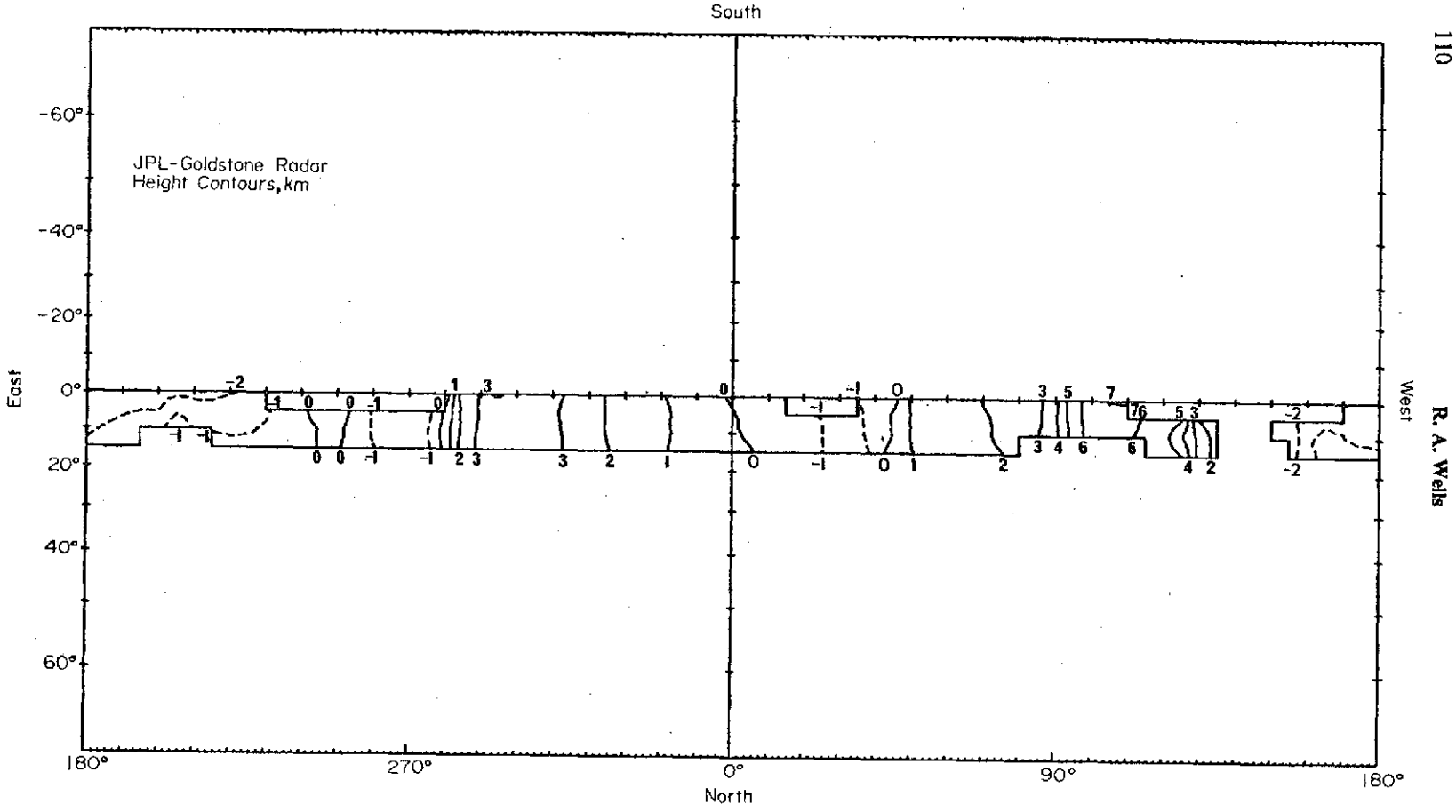

FIG. 6. Height contours of the 5° grid values obtained from the Goldstone data after smoothing with equation (1). As before, solid lines are zero and positive topography and dashed lines are negative topography. Contours are calculated in 1 km intervals from −2 to +7 km. Compare with Fig. 3.

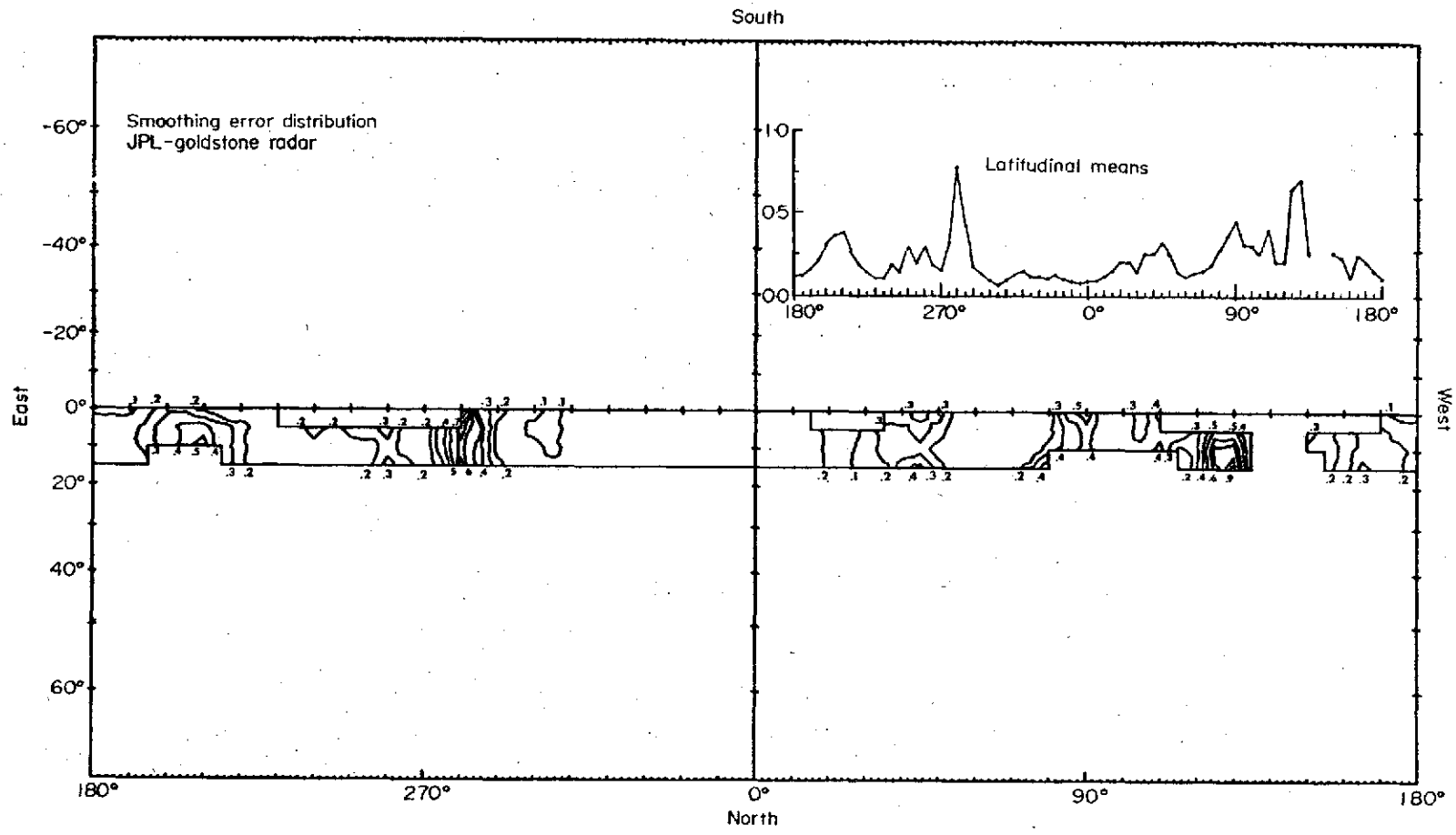

FIG. 7. Contours of the internal smoothing errors $\bar{s}$ derived from equation (2) for the Goldstone data. The contours range from 0·1 to 1·0 km in 0·1 km steps. The diagram at the upper right represents the mean value of $\bar{s}$ with longitude. Large errors are apparently associated with slopes in the topography. Compare with Fig. 4.

Numerical values obtained for p_{CO_2} are derived using the following procedure: Belton & Hunten's (1971) July 1 observations within the rectangle $\pm 15°$ latitude and 320° to 40° longitude were used to calculate a trial value for C assuming that the mean CO_2 pressure for the data points within the rectangle equalled an arbitrary 6 mb. The remainder of the points for that night were then used to give corresponding pressures with this value of C. The constants C for the remaining nights are similarly calculated by using data in overlaps of successive nights. Each mean pressure within an overlap (averaged from points determined by the previous C) provides a new C for that night, and so on. (The distribution of data points including nightly overlaps is shown in Fig. 8.) This procedure gives a series of constants for all of the data, which can then be consistently adjusted until the mean pressure over all observations equals 5·5 mb. This latter pressure value was chosen because the observations of Belton & Hunten (1966) and Belton, Broadfoot & Hunten (1968) indicated that the mean CO_2 pressure for Mars integrated over an appreciable fraction of the disk was 5·5 mb.

This pressure value is an imposed constraint. However, there is no *a priori* reason to believe that the total mean CO_2 pressure for Mars is 5·5 mb since the earlier observations of Belton *et al.* do not cover the entire planet. But with their method, the entire calibration of the Earth-based CO_2 observations is internally self-consistent depending only on ground-based spectroscopy. Comparisons with the Haystack radar data will further elucidate the calibration problems.

Once pressure values have been obtained from equation (3), surface heights can be derived after adopting a particular atmospheric model. The model used here is that of Belton & Hunten (1971). Surfaces of constant pressure in a static, isothermal atmosphere coincide with surfaces of constant gravitational potential; otherwise, violent winds would result. The surface that coincides with a CO_2 pressure of 5·5 mb is chosen to be the gravitational potential surface at zero height. The atmosphere at any point is then taken as isothermal. Diurnal temperature variations are neglected since all observations were made at noon local time on Mars, i.e. along the apparent central meridian. The effective temperature of the atmosphere is, however, latitudinally dependent.

These assumptions, which should be valid at least up to one scale height, permit the isothermal equation

$$p = p_0 \exp[-(z/H)] \tag{4}$$

to be used to derive surface heights z from observed pressures p using 5·5 mb for p_0. The latitudinal temperature dependence is accounted for by calculating the local scale height of the atmosphere for each observation point from $H = kT/mg$ with usual definitions for the gas constants appropriate to CO_2 under Martian gravity. The variation of T with latitude is that adopted from Belton & Hunten (1971) who utilized their previous determination of the rotational temperature of Martian CO_2 (Belton *et al.* 1968) together with the numerical model of latitudinal temperature dependence calculated by Leovy & Mintz (1969). See Belton & Hunten (1971), Fig. 8.

The observation dates were: 2, 22, 23, 24, 30 June and 1 July (B & H 1971); and 9, 10, 11, 12, 13, 14, 15 June (Wells 1969a). The distribution of observational points is given in Fig. 8.

The 1 mm^2 spectrograph entrance aperture was theoretically equivalent to about an 850 km square near the Martian equator. The size and shape of this element varied with seeing conditions and latitude on the planet (see B & H, 1971, Fig. 7). Planetary rotation produced negligible effects since observation times were very short. A mean figure of about 1000 km for the spatial resolution is adopted here since seeing was relatively good (2″–3″ arc) for most nights.

Data co-ordinates, obtained by measuring the x, y positions of the centre of the

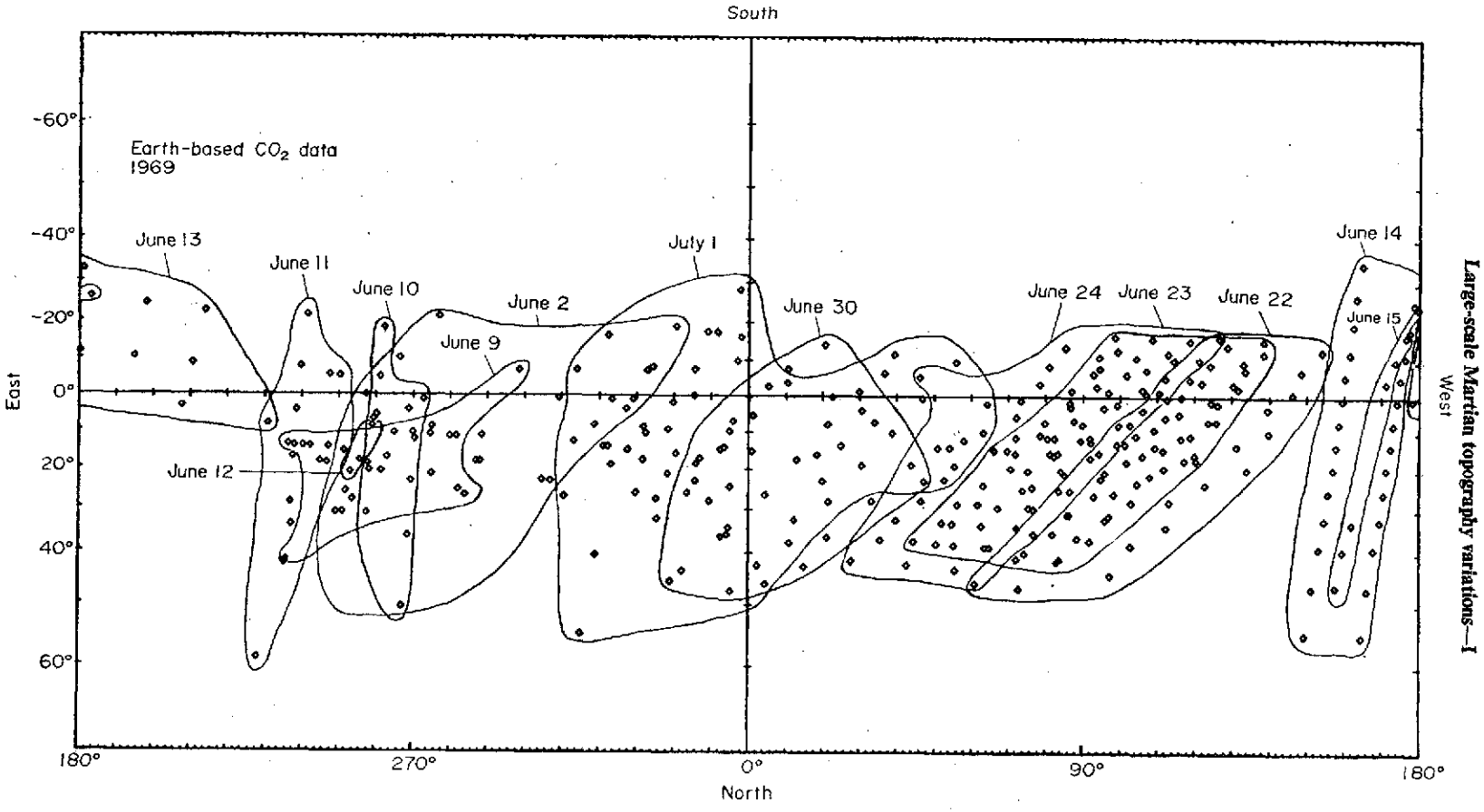

FIG. 8. The distribution of 339 Earth-based Martian CO_2 determinations made at Kitt Peak National Observatory by Belton & Hunten (1969, 1971) and Wells (1969a). Observation dates and the night-to-night overlaps are shown. Note that many overlaps are not well populated and the overlap coverage is not complete for all longitudes. Refer to Fig. 20 for the location of the points on Mars.

aperture on Mars in the guiding reticle relative to the sky, were corrected for displacements caused by dispersive refraction introduced by the Earth's atmosphere (guiding was performed in visual light). The estimated accuracy of these position determinations was about 2 per cent of the diameter of the planet, roughly 140 km (B & H 1971).

The measurements obtained by the writer were reduced simultaneously with those of Belton & Hunten during the summer of 1970 at Kitt Peak National Observatory. The reduced data are presented in Table 1 which represents a continuation of B & H's (1971) Table 4. The altitudes listed in Table 1 refer to a zero level of 5·5 mb. Estimated RMS errors in pressures and heights have been included. They reflect only the random uncertainty in counts obtained in the data channels. These errors are exponentially distributed with height. The general level of precision, except for two nights, is close to ± 1 mb in pressure corresponding to about ± 2 km near zero altitude.

Belton & Hunten (1971) compared their ground-based CO_2 altitudes with the Haystack radar observations and with the Mariner data of Herr *et al.* (1970) to establish the degree of correspondence. Comparisons with the Mariner data at first yielded favourable results (B & H 1971, Fig. 11); however, after the ground-based CO_2 measurements were normalized to the Haystack radar data (described in the following paragraphs), many of the similarities disappeared.

No explanations for these discrepancies were given. Presumably this was because the published data of Herr *et al.* (1970) were re-reduced using new low temperature laboratory data for their 2 μ CO_2 curve-of-growth at about the same time B & H prepared their final report.

Table 1

*Kitt Peak CO_2 reductions of Wells**

Date	Long. (°W)	Lat. (°N = +, °S = −)	Eta	Temp. (°K)	P(mb)	ΔP	Z(km)	ΔZ
69/06/09	236·5	13·7	2·02	200	8·3	1·7–1·6	−4·1	2·2–1·9
	238·1	14·0	2·02	200	8·7	1·8–1·7	−4·6	2·2–1·9
	240·4	14·0	2·02	200	11·0	2·0–1·8	−7·0	1·8–1·7
	242·4	14·0	2·02	200	6·8	1·6–1·5	−2·1	2·5–2·1
	247·3	14·4	2·02	200	8·7	1·8–1·7	−4·6	2·1–1·9
	251·4	15·3	2·03	200	8·1	1·7–1·6	−3·9	2·2–1·9
	237·3	33·9	2·37	192	2·7	1·0–0·9	7·1	4·1–3·2
	251·9	26·0	2·14	196	19·4	2·6–2·3	−12·5	1·3–1·3
	263·1	16·9	2·04	200	13·9	2·2–2·0	−9·4	1·6–1·5
	275·1	8·6	2·05	200	13·0	2·1–1·9	−8·7	1·7–1·6
	282·1	25·4	2·13	196	1·6	0·9–0·8	12·6	6·9–4·6
69/06/09	284·0	26·7	2·15	196	1·0	0·8–0·7	17·2	11·0–6·0
69/06/10	257·6	31·2	2·21	193	0·6	0·3–0·2	22·7	5·6–3·8
	257·9	18·8	2·06	199	4·2	0·5–0·5	2·8	1·3–1·1
	259·3	6·7	2·01	200	16·9	1·0–0·9	−11·4	0·5–0·6
	261·3	−5·1	2·06	200	4·9	0·5–0·5	1·3	1·2–1·0
	262·2	−18·4	2·22	199	7·3	0·6–0·6	−2·7	0·9–0·8
	267·2	50·5	2·81	183	4·2	0·4–0·4	2·5	1·0–0·9
	268·6	36·3	2·33	191	8·1	0·6–0·6	−3·7	0·8–0·7
	269·4	23·4	2·11	197	12·8	0·8–0·7	−8·4	0·6–0·6
	270·6	12·1	2·03	200	10·3	0·7–0·7	−6·3	0·8–0·7
69/06/10	272·9	1·3	2·03	200	6·7	0·6–0·6	−2·0	1·0–0·9
69/06/11	228·1	58·9	3·30	177	19·5	0·9–0·8	−11·3	0·4–0·4
	235·6	42·2	2·48	188	11·0	0·8–0·7	−6·6	0·6–0·6
	237·1	28·7	2·17	195	10·7	0·8–0·7	−6·5	0·7–0·7
	237·8	16·9	2·04	200	17·4	1·0–0·9	−11·6	0·5–0·6

Date	Long. (°W)	Lat. (°N = +, °S = −)	Eta	Temp. (°K)	P(mb)	ΔP	Z(km)	ΔZ
69/06/11	238·6	4·4	2·01	200	19·1	1·1 –1·0	−12·6	0·5 –0·6
	239·8	−7·8	2·08	200	13·5	0·9 –0·8	−9·1	0·6 –0·6
	241·6	−21·6	2·28	198	8·8	0·7 –0·7	−4·6	0·8 –0·7
	245·0	18·1	2·05	199	3·3	0·5 –0·5	5·2	1·5 –1·4
	246·8	18·5	2·06	199	3·4	0·5 –0·5	5·1	1·5 –1·3
	247·7	−5·7	2·06	200	8·7	0·7 –0·7	−4·6	0·9 –0·8
	250·4	−5·3	2·06	200	7·4	0·6 –0·7	−2·9	0·9 –0·8
69/06/11	253·2	21·1	2·08	198	1·3	0·4 –0·3	14·5	2·9 –2·4
69/06/12	253·7	27·8	2·18	195	5·7	2·1 –1·8	−0·4	3·8 –3·1
	255·8	18·0	2·07	199	14·2	3·2 –2·9	−9·6	2·3 –2·1
69/06/12	259·2	8·8	2·05	200	4·7	2·0 –1·7	1·7	4·6 –3·6
69/06/13	178·2	0·7	2·02	200	5·2	3·4 –2·7	0·7	7·4 –5·1
	180·4	−11·8	2·12	200	18·5	5·8 –5·0	−12·3	3·2 –2·8
	183·3	−26·1	2·39	196	5·6	3·2 –2·6	−0·1	6·1 –4·5
	194·9	−10·5	2·10	200	25·5	6·8 –5·9	−15·5	2·7 –2·4
	198·1	−24·6	2·35	197	11·7	4·5 –3·7	−7·5	3·8 –3·2
	207·6	3·2	2·02	200	6·9	3·8 –3·1	−2·3	6·0 –4·5
	210·7	−8·8	2·09	200	12·9	4·9 –4·1	−8·6	3·9 –3·3
	214·0	−22·7	2·31	197	31·9	7·3 –6·4	−17·6	2·2 –2·1
69/06/13	230·9	8·1	2·02	200	14·8	5·4 –4·5	−10·0	3·7 –3·1
69/06/14	149·5	55·0	3·05	180	0·9	0·2 –0·2	16·3	2·5 –2·0
	151·4	46·8	2·64	185	2·0	0·3 –0·3	9·5	1·6 –1·4
	153·2	38·8	2·38	190	3·3	0·4 –0·4	4·9	1·2 –1·1
	154·8	32·3	2·24	193	5·2	0·5 –0·5	0·7	1·0 –0·9
	155·7	25·7	2·13	196	6·8	0·6 –0·6	−2·0	0·9 –0·8
	157·1	19·7	2·07	199	7·4	0·6 –0·6	−2·9	0·9 –0·8
	157·8	13·4	2·03	200	9·3	0·7 –0·7	−5·3	0·8 –0·7
	158·5	7·2	2·01	200	10·0	0·7 –0·7	−6·0	0·8 –0·7
	159·6	0·5	2·02	200	11·6	0·8 –0·7	−7·6	0·6 –0·7
	160·1	−5·9	2·06	200	17·4	0·9 –0·8	−11·6	0·5 –0·5
	161·4	−12·1	2·12	200	19·6	1·0 –0·9	−12·8	0·5 –0·5
	162·6	−19·5	2·24	199	17·8	0·9 –0·8	−11·8	0·5 –0·5
	163·4	−26·9	2·41	196	15·7	0·8 –0·7	−10·4	0·5 –0·5
	164·8	−34·6	2·67	192	18·4	0·9 –0·8	−11·7	0·4 –0·4
	164·6	55·3	3·07	180	8·4	0·6 –0·5	−3·8	0·6 –0·6
	166·1	47·1	2·66	185	11·8	0·7 –0·6	−7·1	0·5 –0·5
	167·9	39·0	2·39	189	14·5	0·8 –0·7	−9·2	0·5 –0·5
	169·6	32·5	2·24	193	18·7	1·0 –0·8	−12·0	0·4 –0·5
	170·6	26·0	2·14	196	21·9	1·0 –0·9	−13·7	0·4 –0·5
	171·3	19·6	2·07	199	22·4	1·1 –0·9	−14·1	0·4 –0·5
	172·5	13·7	2·03	200	18·9	1·0 –0·9	−12·5	0·5 –0·5
	173·2	7·5	2·01	200	13·5	0·8 –0·8	−9·1	0·6 –0·6
	174·1	1·2	2·02	200	10·3	0·7 –0·7	−6·3	0·7 –0·7
	175·0	−5·1	2·05	200	11·2	0·8 –0·7	−7·2	0·6 –0·7
	176·4	−11·3	2·11	200	10·1	0·7 –0·7	−6·2	0·7 –0·7
	177·6	−18·1	2·21	199	4·9	0·5 –0·5	1·3	1·1 –1·0
	178·9	−25·4	2·37	196	4·0	0·4 –0·4	3·2	1·1 –1·0
69/06/14	181·1	−32·9	2·61	193	9·4	0·6 –0·6	−5·2	0·6 –0·6
69/06/15	157·7	46·6	2·64	185	39·2	8·9 –7·8	−18·4	2·1 –1·9
	159·5	39·2	2·40	189	17·4	6·3 –5·2	−11·0	3·4 –3·0
	162·2	33·1	2·26	192	6·0	4·0 –3·1	−0·7	7·1 –5·0
	171·3	−4·1	2·05	200	8·7	4·8 –3·8	−4·5	6·0 –4·5
	173·8	−10·2	2·10	200	13·0	5·7 –4·7	−8·7	4·5 –3·7
	176·6	−16·6	2·19	200	4·1	3·4 –2·6	3·0	9·9 –6·2
69/06/15	179·8	−24·4	2·35	197	6·9	4·1 –3·2	−2·2	6·3 –4·6

* Belton & Hunten's (1971) Table 4 contains their observations.

The net effect of these new reductions, however, was a lowering of the Mariner IRS altitudes by about 3 km. Nevertheless, a straightforward comparison of the Mariner IRS data with the currently available ground-based measurements is probably not significant since the Mariner scans are located at the extreme limits of B & H's (1971) measured points. At the locations where there are scan crossings by the two data sources, only a few points are available in each set through which to construct smooth height-trend curves. (The treatment of the Mariner IRS zero level is discussed in the next section.)

Comparisons between the Haystack data and the ground-based CO_2 measurements introduced a serious conflict. Fig. 12 in B & H's (1971) report shows a major discrepancy in altitude between 80°–110° W longitude (much lower altitudes for the ground-based CO_2 measurements than for the Haystack radar data), although they noted that '... (i) the zero height levels are effectively identical; thus the radar results support the 1967 and 1969 spectroscopic results which give a 'planetary mean' partial pressure of 5·5 mb. (ii) The overall *trend* in topographic variation (except between 80° and 110° W) is roughly the same. Note in particular that the slopes in all regions except 80°–110° W are very similar. (iii) The linear scale of topographic features is effectively the same for both sets of data ...'.

The most probable cause in the altitude discrepancy at 80°–110° W was suggested by B & H (1971) to be due to problems in the night-to-night determinations of the constant C in equation (3). There are two significant error sources in the determination of C: (1) the data points do not thoroughly cover a complete circuit of the planet; and (2) not every overlap contains a large number of observations (see Fig. 8, this report). Thus, this method of overlap calibration can propagate errors throughout the whole series of observations and can readily lead to distortions in the data curves of height vs. longitude. B & H (1971) considered these factors to be the likely cause of the altitude discrepancy and therefore resorted to a normalization of their measurements to those of the Haystack observations.

Appending the unnormalized reductions of Table I to those in B & H's (1971) Table 4, the writer has followed a similar procedure in preparing the ground-based CO_2 measurements for the combination with other sources. Certain differences in the calculations from those used by B & H (1971), however, will be noted.

A resolution equivalent to a 1000 km diameter circle (18° on the planet) was used in equations (1) and (2). Fig. 9 (top) indicates that the standard deviations in altitude cannot be used as weighting factors since they are distributed exponentially with height; thus negative topography would always be preferentially weighted more than positive topography. However, the observational precision also depends on the airmass factor η, the geometrical pathlength through the Martian atmosphere. Fig. 9 (bottom) shows a plot of airmass values against associated ground-based CO_2 altitudes. Since the distribution is random, the weighting factor in equations (1) and (2) can be defined as $w_i = 1/\ln(\eta_i)$. This relationship arises since eq. (3) indicates that pressure is a function of the airmass and pressure and altitudes are logarithmically related by equation (4). (In their smoothing calculations, B & H (1971) used only the gaussian filtering function. No other weighting was attempted.)

Equation (1) yielded 530 5°-grid values from the combined 339 points of B & H (1971) and Wells (1969a). A comparison was then made with the Haystack radar results. Fig. 10, curve A, shows the mean CO_2 curve averaged between 0° and 25° N latitude from the smoothed data compared to all of the Haystack data between 0° to 21° N latitude at the original radar resolution of 300 km. B & H's (1971) curves in their Fig. 12 range from 240°–0°–120° W longitude. The curve shown in Fig. 10 has been extended from 240° W to 230° W and from 120° W to 180° W. The discrepancy noted by B & H (1971) between 80°–110° W is seen in Fig. 10 between 80°–180° W. There is a similar, though smaller, discrepancy between 230°–280° W. Between 280° W and 80° W, however, the ground-based data shown in Fig. 10 fit the radar data in slope and

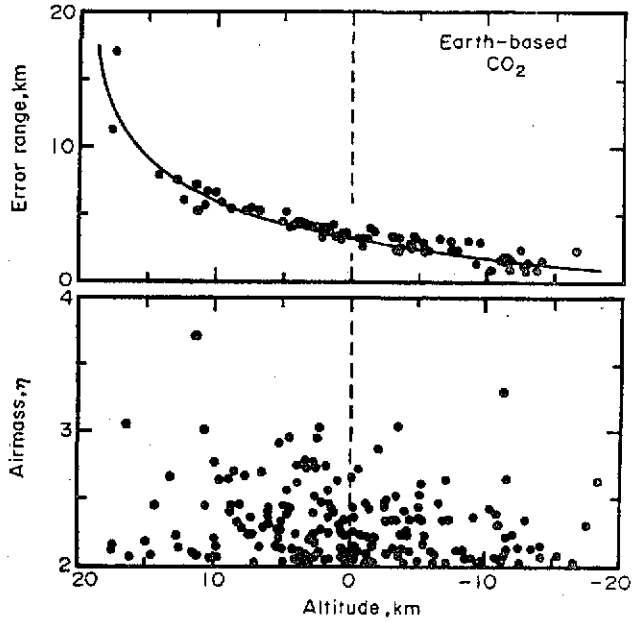

FIG. 9. Upper: The error range range (sum of the absolute values of the ± standard deviations) plotted against altitude for the Earth-based CO_2 observations. Note the clearly defined exponential relationship of increasing error with increasing height. Lower: A plot of the airmass factors of the Earth-based CO_2 measurements against altitude. The distribution is random.

zero level very well. (Note: the large values for the CO_2 altitudes given by the dotted line near 300° W are not considered seriously discordant because of an exponential loss of instrumental sensitivity with increasing height, cf. Fig. 9, top.)

Curve B is the height variation of the CO_2 observations after normalization to the radar data. The normalization procedure was as follows. The CO_2 observations for for each night were compared to the Haystack radar data in the corresponding longitude interval between the latitudes 0° and 25° N. There are 13 longitude intervals for the 13 nights of observations. Only those CO_2 data within the given latitude limits were averaged together. The radar data within the same co-ordinate rectangle were also averaged. The difference between the two averages represents the correction to all of the CO_2 measurements for that night. In this way, CO_2 data outside the given latitudinal limits are also adjusted. This procedure is different from that of B & H (1971) who used only the radar measurements between latitudes 9·1° and 12° N for the night-to-night corrections to all of their CO_2 data.

Table 2 lists values for the normalization of all the ground-based CO_2 data as described above in the author's procedure.

The remaining discrepancies after normalization between 230°–240° and at 300° W do not seriously affect the final data combination since the data points involved have very low weights.

There may be some question concerning the raised flatland near 150° W. There is a suggestion of this feature in the radar data although not as pronounced as in the CO_2 observations. Most of the CO_2 points in this region have large errors associated with them as will become apparent in the following paragraphs.

The 530 values produced by equation (1) were adjusted by the parameters listed in Table 2. A contour plot of the normalized heights is given in Fig. 11. This contour map is somewhat more conservative than that given by B & H's (1971) Fig. 15 even

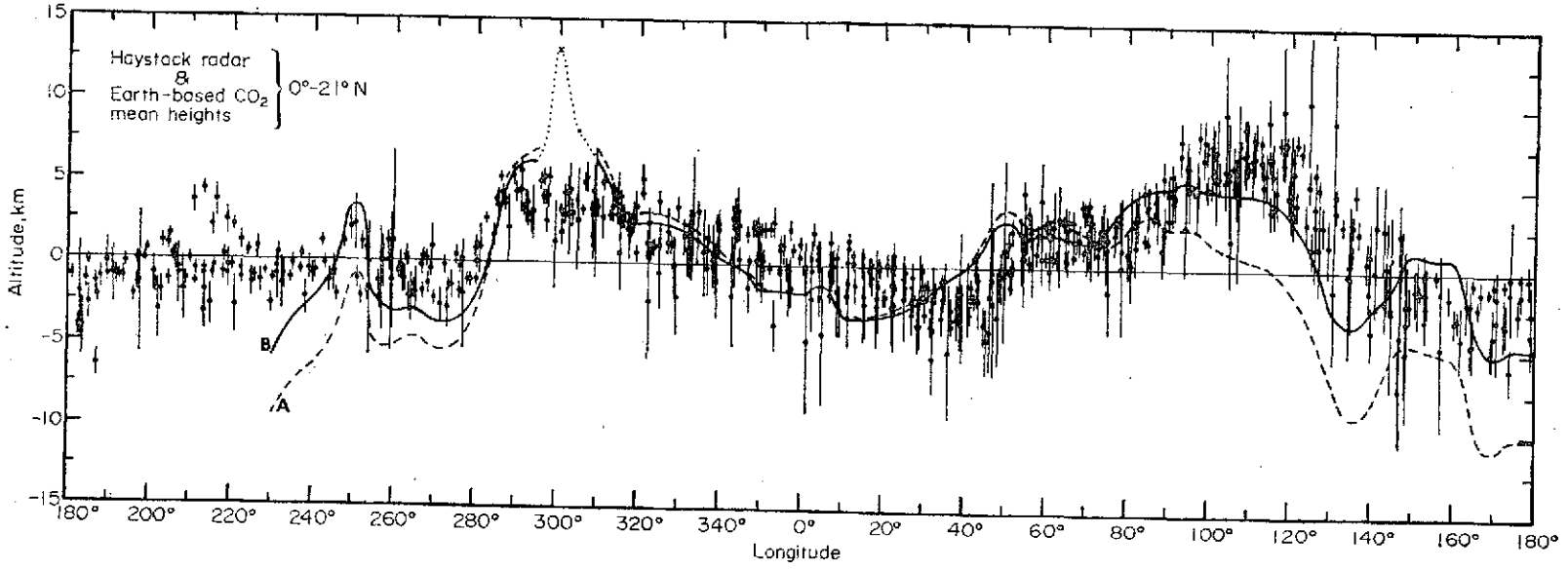

FIG. 10. Comparison of Earth-based mean CO_2 heights with all of the Haystack radar data between about 0° and 21° N latitude. The Haystack data are at the original resolution of 300 km and the error bars represent one standard deviation. Curve A is the average between 0° to 25° N of the smoothed ground-based CO_2 data. The curve is calculated on 5° intervals at 1000 km resolution and is unnormalized to the radar data. Curve B is the same curve after normalization to the radar data as explained in text. The discrepancy shown by the dotted line near 300° W is not considered seriously discordant because of the exponential loss of instrumental sensitivity to height with increasing height.

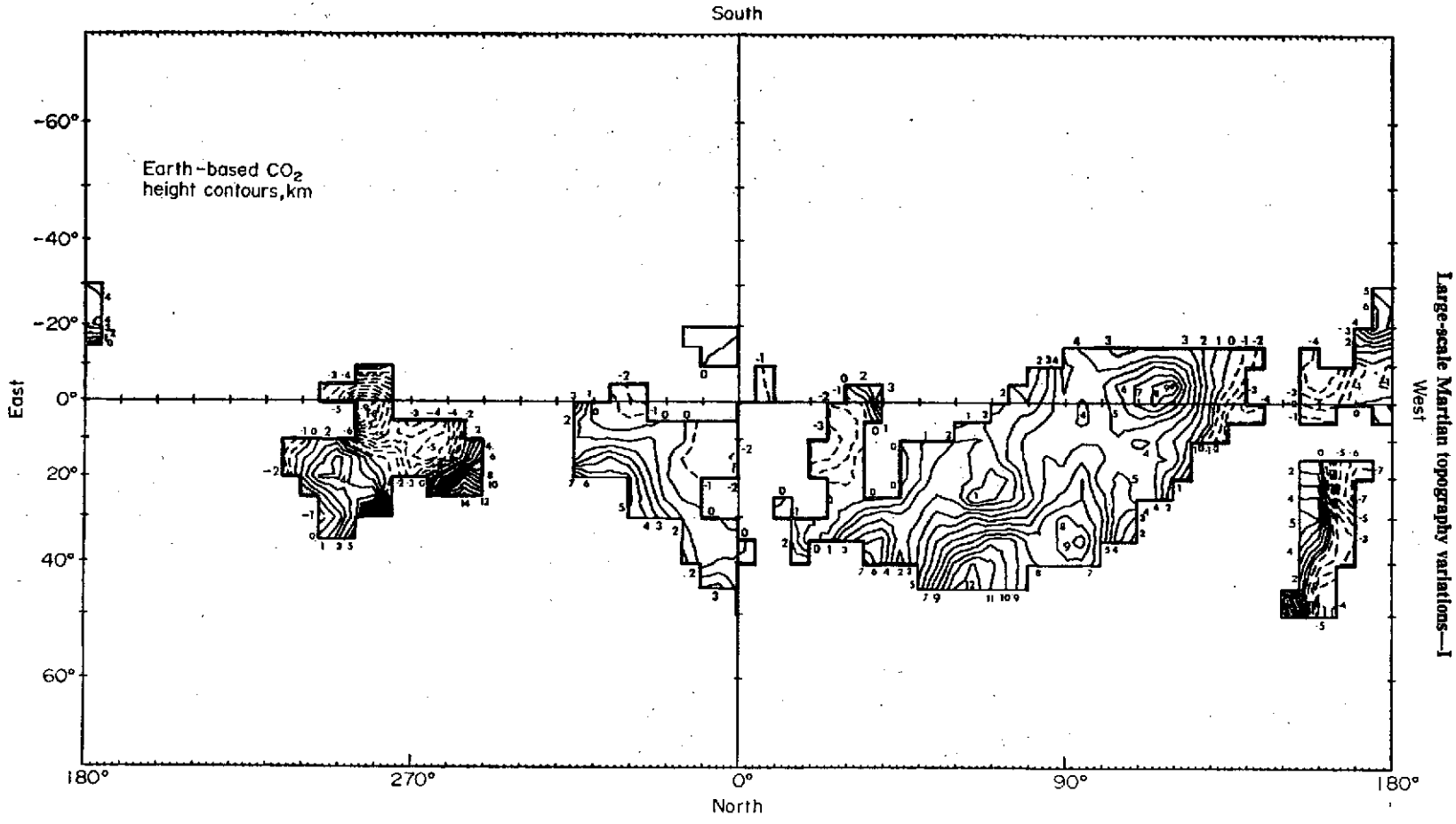

FIG. 11. Height contours of the normalized ground-based CO_2 measurements of Martian altitudes after smoothing with equation (1). The contour range is from −9 to +14 km in 1-km intervals. Solid lines represent zero and positive topography, while dashed lines represent negative topography. This map is more conservative than Fig. 15 of Belson & Hunten (1970) since the smoothing programme rejected grid values if there were fewer than three data points within a resolution element.

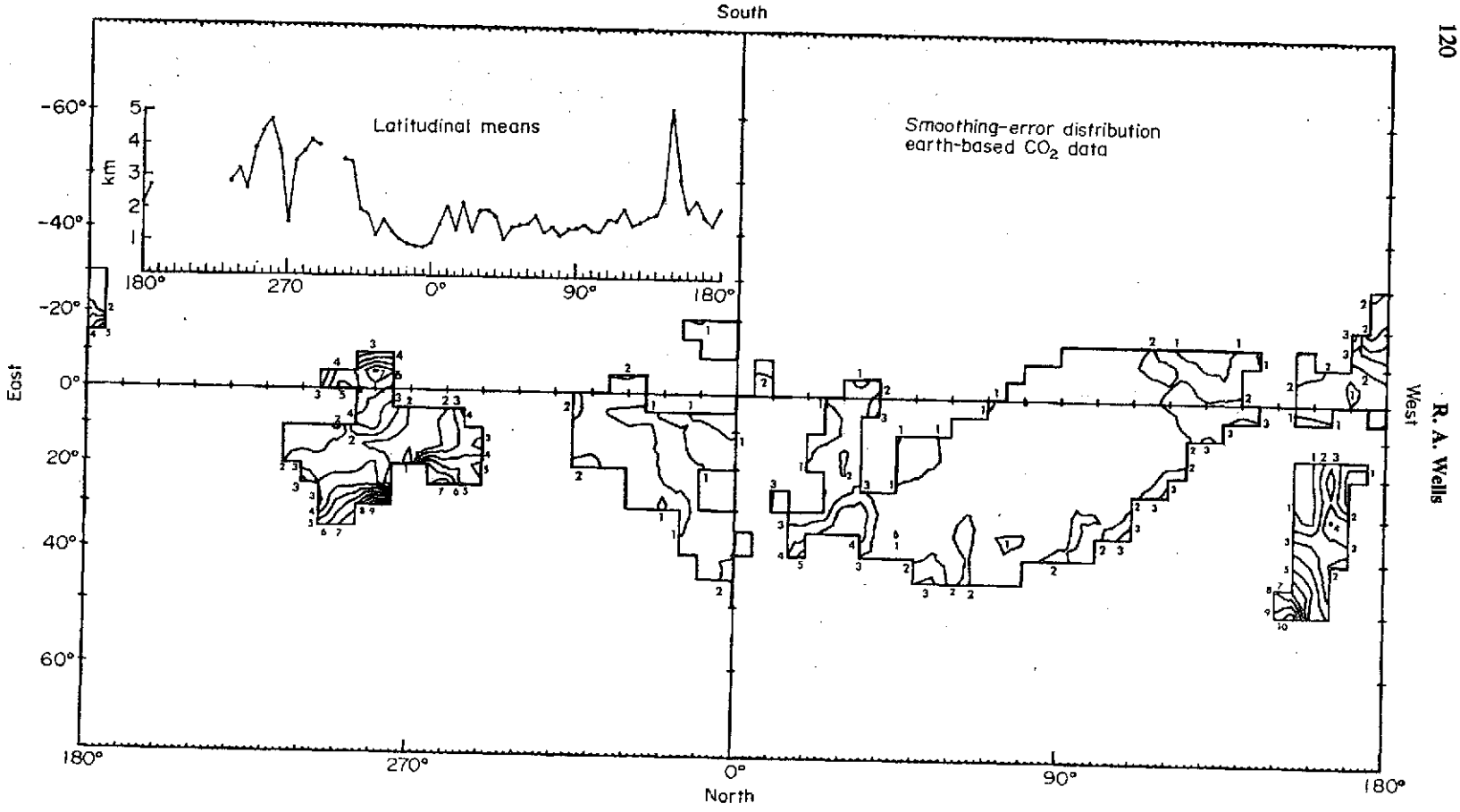

FIG. 12. Contours of the internal smoothing errors $\bar{s}$ derived from equation (2) for the ground-based CO_2 determinations. The errors range from 1 to 10 km in 1-km intervals. The distribution of the mean of $\bar{s}$ with longitude is given in the upper left diagram. The largest errors are associated with slopes and regions where the original data had large deviations, notably near 260°, 280°, and 150° W.

Table 2

Normalization parameters for the Kitt Peak CO_2 data

Date	Longitude (W)	$\bar{Z}$ (radar) (km)	No. Pts.	$\bar{Z}$ (CO_2) (km)	No. Pts.	CO_2 shift (km)
Belton & Hunten Data						
69/06/02	235°–0°–16°	0·91	258	1·58	22	−0·67
69/06/22	60°–155°	3·27	206	−2·49	17	5·76
69/06/23	52°–139°	3·78	196	0·76	30	3·02
69/06/24	27°–113°	1·74	215	2·66	21	−0·92
69/06/30	329°–0°–44°	−0·58	182	−0·83	12	0·25
69/07/01	310°–0°–65°	0·02	270	0·32	22	−0·30
Wells Data						
69/06/09	236°–286°	−0·35	74	−5·55	8	5·20
69/06/10	257°–273°	−0·78	28	−5·06	5	4·28
69/06/11	228°–254°	−0·44	34	−3·48	5	3·04
69/06/12	253°–260°	−0·37	13	−3·95	2	3·58
69/06/13	178°–238°	−0·86	93	−3·87	3	3·01
69/06/14	150°–188°	−2·14	56	−7·97	8	5·83
69/06/15	155°–180°	−2·27	35	(−7·97)*	(8)*	5·70

* Determined from preceding line since there were only CO_2 points outside the latitudinal limits 0°–25° N in this longitudinal interval.

with the writer's data included. The blank areas in Fig. 11 between about 270°–340° W and at the centre near 10°–20° W resulted because the smoothing program yielded grid values only if at least three data points were within the resolution circle. These regions are contoured in B & H's (1971) map.

Associated with these contours, the internal smoothing errors $\bar{s}$ are shown in Fig. 12. The errors range from 1 to 10 km in 1 km steps. Areas with the smallest smoothing errors are those between 315°–0° W and 45–145° W longitude. The largest errors are located wherever there are very steep slopes leading from altitudes higher than about 10 km, e.g. 260° W, 280° W, and 150° W. The region near 150° W reflects a large internal error due to poor data, as was previously mentioned. A chief value in the smoothing-error contour plots is to quantitatively depict just those areas that are the most suspicious.

The technique of measuring surface heights on Mars by groundbased CO_2 spectroscopy is in fact a valuable one. An electronically stable and permanent instrumental set-up is, however, mandatory to avoid efficiency changes each time the equipment is taken down and to avoid the rather large errors that can accumulate in the raw data counts as was evident in the June 13 and 15 observations (Table 1) by the writer. It is also necessary to maintain a careful and well populated overlap coverage in the observations in order to insure an accurate determination of C in equation (3).

These points have been kept in mind for the observations conducted with new instruments at Cerro Tololo, Chile during the 1971 apparition of Mars.

5. Mariners 6 and 7 Infrared spectrometer CO_2 data

In addition to the various analyses of reflection spectra performed on the Mariner 6 and 7 IRS data, CO_2 pressures derived from absorptions near 2 μ were obtained by Herr *et al.* (1970) for the purpose of deducing surface heights along limited scan paths on Mars.

This spacecraft method of CO_2 spectroscopy has the distinct advantage of very

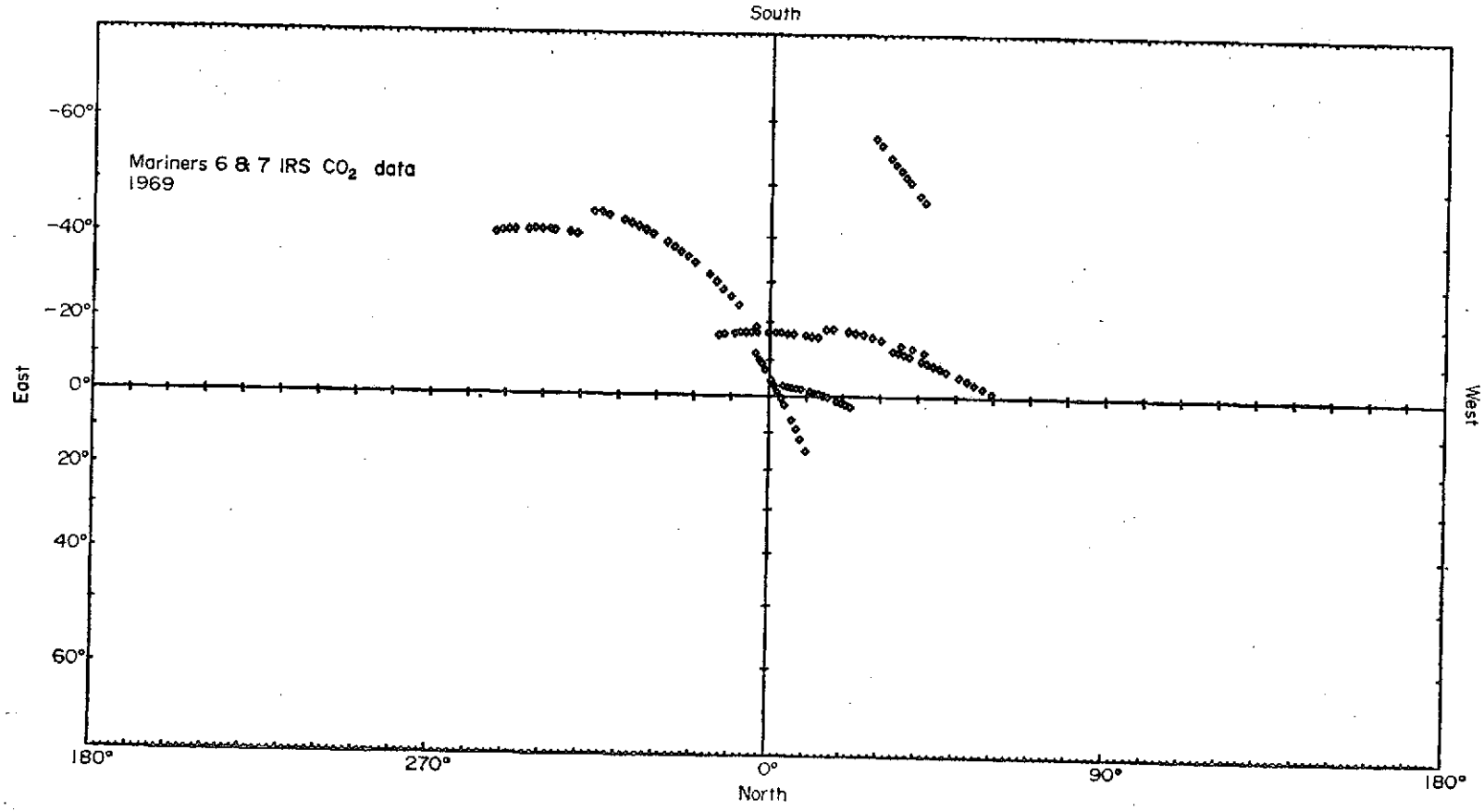

FIG. 13. Distribution of 107 points measured by the Mariner 6 and 7 Infrared Spectrometer experiments (Herr *et al.* 1970) in the 2 μ band of CO_2 during the close approaches to Mars in August 1969. A total of 16 points have been omitted from the published data because of associated large airmass values. Refer to Fig. 20 for the location of the distribution on Mars.

high spatial resolution. It suffers the disadvantage of very limited scan paths across the surface. The distribution of points on Mars used in this section is given in Fig. 13 (16 points were omitted: those listed as questionable by the experimenters and seven additional ones by this writer, explained shortly). The resolution of these observations is equivalent to a rectangle on the surface of approximately 130×8 km determined by the spacecraft motion (8 km) and the optical properties of the instrument (130 km).

A check between absolute heights from the Mariner data and those from the Haystack measurements indicated significant differences. (The Mariner data used here are those obtained with the new low temperature curve-of-growth and not the values published by Herr *et al.* (1970). The new values were generously supplied to the author.) It was therefore necessary to normalize the Mariner data to the radar data. Since this was the case, there was no need to alter the experimenters' originally adopted zero altitude level which corresponded to 6·0 mb. The normalization automatically accounts for zero level shifts.

Part of the Mariner scans were at high latitudes so that a correction also had to be made for the latitudinal temperature dependence of the atmosphere (the Mariner IRS experimenters assumed a constant 200°K for the atmospheric temperature). This correction was accomplished with the aid of equation (8) in the report by Herr *et al.* (1970). By ratioing this equation with itself using different subscripts on the variables representing the constant temperature case and the variable temperature case, corrected altitudes were defined as

$$Z_1 = H_1\{(Z_0/H_0) - \tfrac{1}{2} \ln [(H_0/H_1)(T_1/T_0)^{\frac{1}{2}}]\}, \tag{5}$$

where '0' subscripts refer to the original parameters by Herr *et al.* (1970) and the '1' subscripts represent the parameters associated with the varying temperatures. The original values were $H_0 = 10$ km, $T_0 = 200°$ K, and $Z_0 =$ the tabulated heights. New temperatures and scale heights were calculated for each Z_0 according to the description given in Section 4.

The final adjustment included a shift of the Mariner altitudes to those of the Haystack data. Fortunately, both Mariner tracks crossed or were very close to portions of the radar scans. Mariner 6 had two overlaps, but the scan between 30°–80° W longitude and −13° S to about 7° N latitude had only four points near a radar scan, three of which were omitted because of airmass values greater than 3·8 (explained shortly). The other Mariner scans were located in the region 10°–30° W, −2° S to 3° N (M6) and 0°–10° W, 0°–14° N (M7).

The simplest adjustment factor is the difference in the means between the Mariner and radar data in the areas mentioned above. For Mariner 6, the measurements do not actually cross the nearest radar scans; however, a 9°-radius circle centred at 2° N, 20° W contained 18 radar points and eight Mariner points. For Mariner 7, the observations do cross the radar scan paths. A 9°-radius circle centred at 7° N, 6° W contained 30 radar points and six Mariner points. Data outside these circles were considered to be too far away to be included in the average. The parameters calculated from these two groups are given in Table 3.

An interesting consequence of this normalization is the 0·68 km larger adjustment to the radar data necessary for Mariner 7 than for Mariner 6 (Table 3, column 4). This difference in data shifts suggests a difference between the performances of the two spectrometers and nicely confirms a similar observation of Herr *et al.* (1970). Their Fig. 2 shows the 2 μ CO_2 bands observed in the same area of Sinus Meridianii by Mariner 6 and 7. Mariner 6 yielded a slightly higher altitude by 0·5 km for the region than did Mariner 7.

The Mariner investigators quoted a 0·5 km error limit as typical of all their altitude measurements. This limit was determined from the possible fits of the continuum across the dips in their spectra. The tabulated airmasses, however, provide the same

Table 3

*Normalization parameters for mariners 6 and 7 IRS CO_2 altitudes**

No. Pts.	Mean height (km)	Mariner shift (km)	Difference (M7–M6)
18	$\bar{Z}$ (radar), −1·76	1·68 (M6)	0·68 km
8	$\bar{Z}$ (M6), −3·44		
30	$\bar{Z}$ (radar), −0·46	2·36 (M7)	
6	$\bar{Z}$ (M7), −2·82		

* These parameters are calculated from unpublished corrections by low temperature laboratory curve-of-growth measurements at 2μ. The corrections were supplied to the author by K. C. Herr.

type of weighting function as utilized in the ground-based CO_2 measurements. Several of the slant paths from the spacecraft were quite large and a check was first made for possible functional relationships between airmass and altitude. Fig. 14 shows such a plot for both Mariners 6 and 7. Since it was evident that there was indeed a cut-off limit above which altitudes increased in value with increasing airmass, all of the low airmass data were not plotted in this diagram for sake of clarity (these are given in the next fig.). The cut-off limits are shown by the vertical lines in Fig. 14. Altitudes for airmasses greater than about 3·8 from Mariner 6 and about 4·6 from Mariner 7 were excluded from this analysis as unreliable. Reasons for the differences in these cut-off values are not apparent.

The plot of altitude vs. airmass for airmasses smaller than the above limits is given in Fig. 15 which shows no evident correlation. The weighting function for equations (1) and (2) is therefore defined as in the previous section, $w_i = 1/\ln(\eta_i)$.

The 107 points in Fig. 13 yielded 148 points on the 5°-grid calculated by equation (1). Fig. 16 shows the resulting contour plot from these values. The notable features are the basin in Hellas (300° W) and the slope towards Noachis which corresponds to Hellespontus. The isolated contour region between 20°–40° W and −50°S to −60° S is marked at 1 km. In the original data (Herr *et al.* 1970), there was some topographical variation along the track, but this was smoothed out by equation (1).

The distribution of $\bar{s}$ associated with these values is given in Fig. 17. The error limits range between 0·1 to 0·6 km in 0·1 km steps, the largest errors occurring in the region of the Hellas-Hellespontus slope. A common feature between the four distributions of $\bar{s}$ shown in Figs 4, 7, 12 and 17 is that the largest internal errors appear to be associated with topographical slopes.

6. Combination of the four data sources

The four data groups, discussed in the previous sections, were each processed by equation (1) and (2) after adjustments were made to the Haystack radar zero level. Each source is therefore available on a 5°-grid interval prepared at a spatial resolution corresponding to a circle of about 1000 km in diameter centred at each point. The data groups are simply combined by using equation (1) again on all the smoothed sources simultaneously. The weight factors are now defined by $w_i = 1/\bar{s}_i^2$ since $\bar{s}$ is consistent between the groups as was mentioned in Section 2.

The distribution of all data points is shown in a single plot, Fig. 18. These 1382 points yielded 1366 numbers for the total of the 5°-grid smoothed sources which, in turn, has resulted in 924 values for the combined regular array. Some information

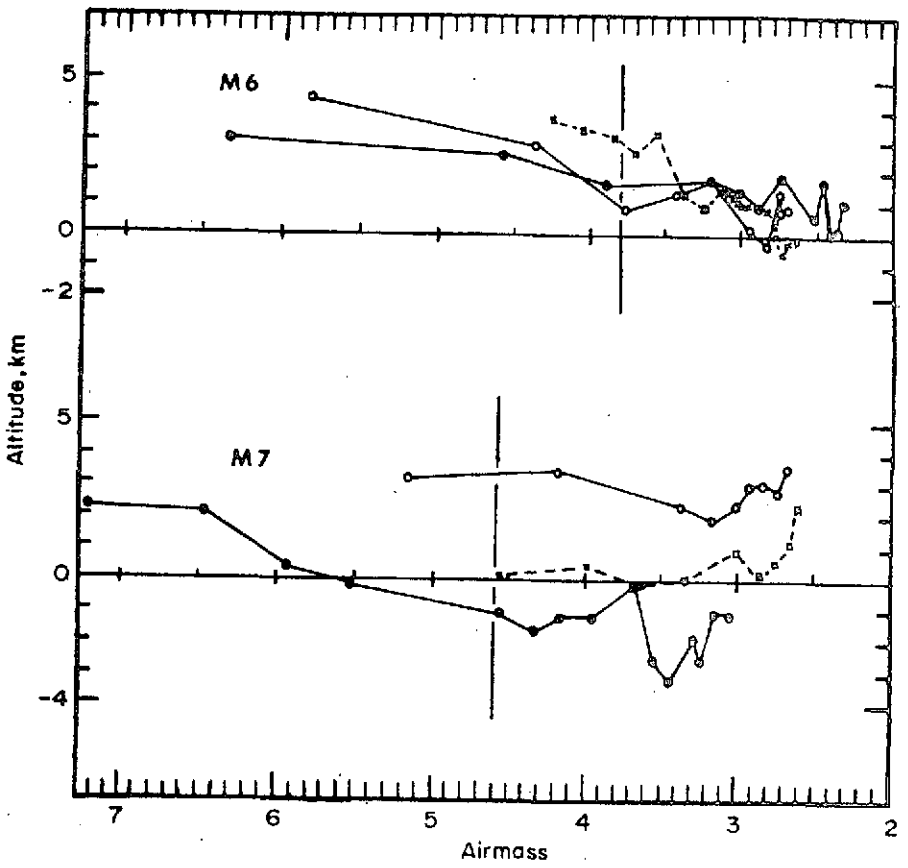

FIG. 14. A plot of measured altitudes against corresponding airmass factors for the Mariner 6 and 7 IRS CO_2 data. The vertical lines at 3·8 and 4·6 represent an approximate cut-off limit placed by the writer. Data above these limits tended to show increasing height with increasing airmass and were therefore omitted from the smoothing calculations. Different symbols merely identify individual scans.

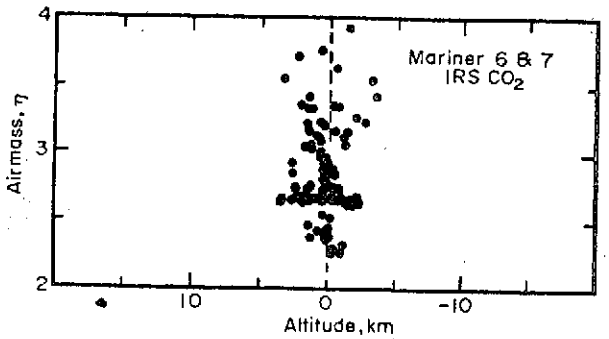

FIG. 15. The distribution of altitudes vs. airmass factors for the Mariner 6 and 7 IRS CO_2 measurements with airmasses smaller than 3·8 (M6) and 4·6 (M7). The distribution is random.

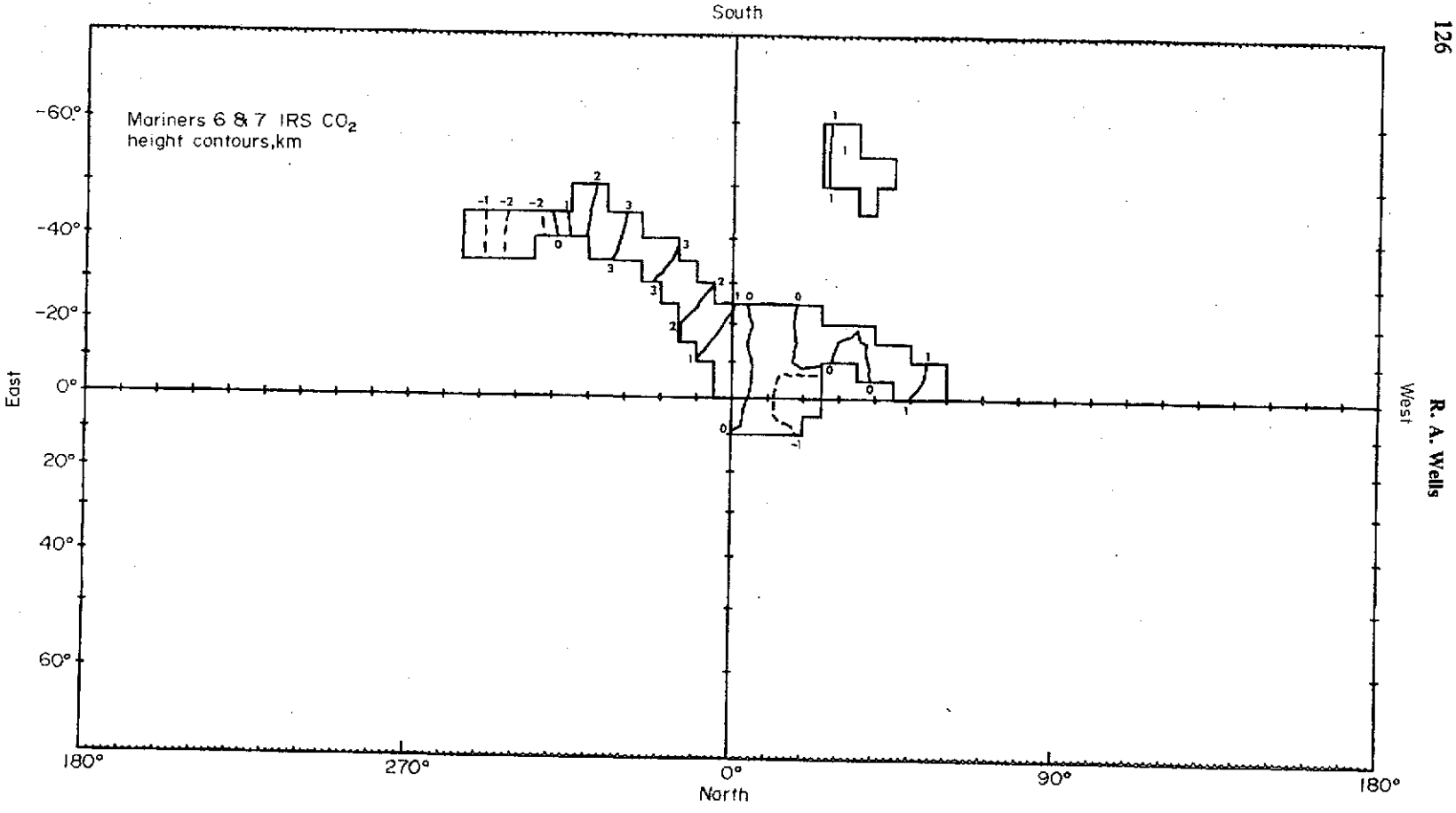

FIG. 16. Altitude contours from the Mariner 6 and 7 IRS CO_2 measurements after smoothing with equation (1). The contours range from -2 to $+3$ km in 1-km intervals. Solid lines represent zero and positive topography, while dashed lines correspond to negative topography.

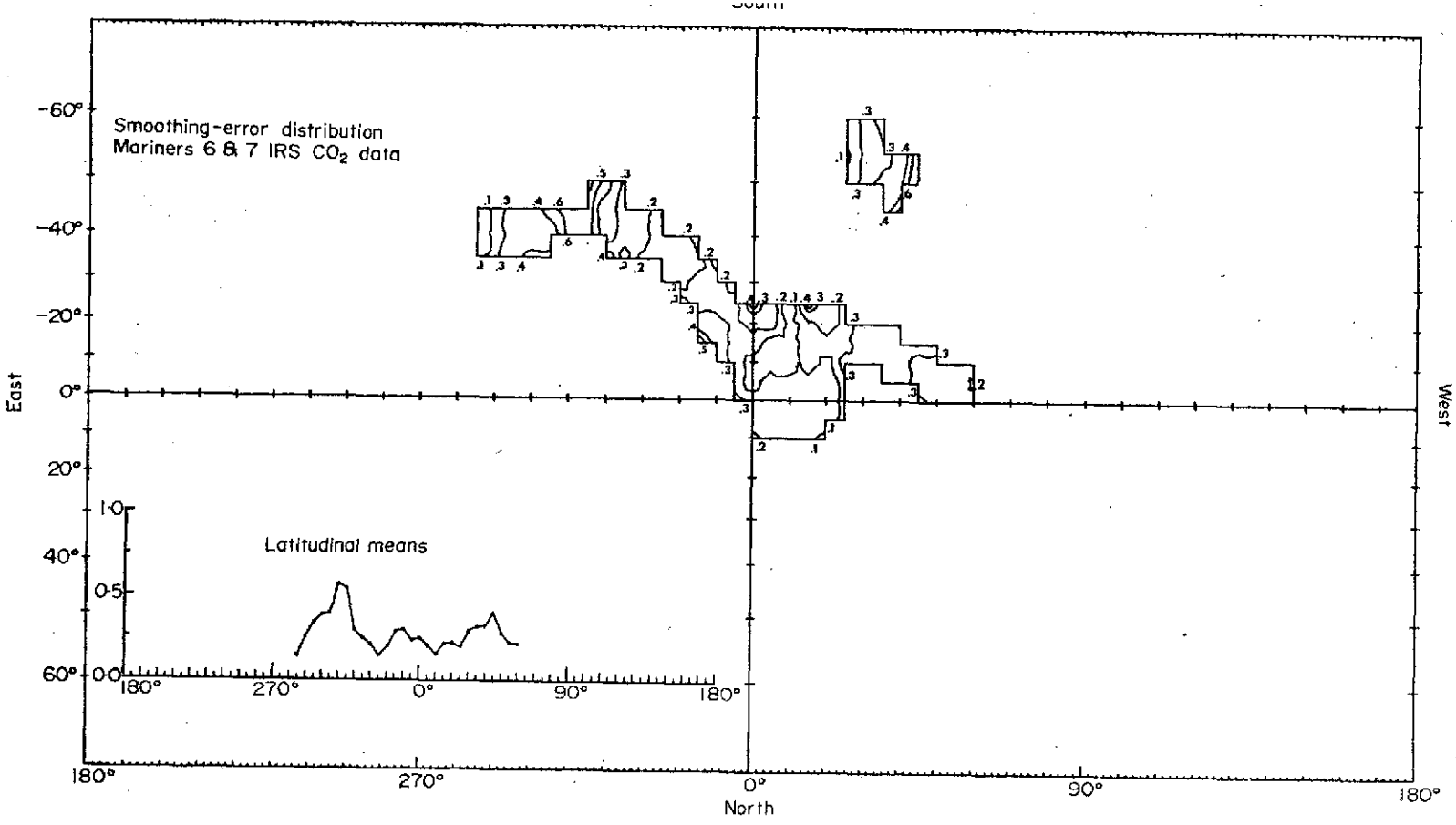

FIG. 17. Contours of the internal smoothing errors $\bar{s}$ derived from equation (2) for the Mariner 6 and 7 IRS CO_2 height determinations. The contours range from 0·1 to 0·6 km in 0·1-km intervals. A plot of the mean value of $\bar{s}$ with longitude is given in the lower left diagram. The largest errors are associated with the slopes in the Hellas–Hellespontus region (31° W).

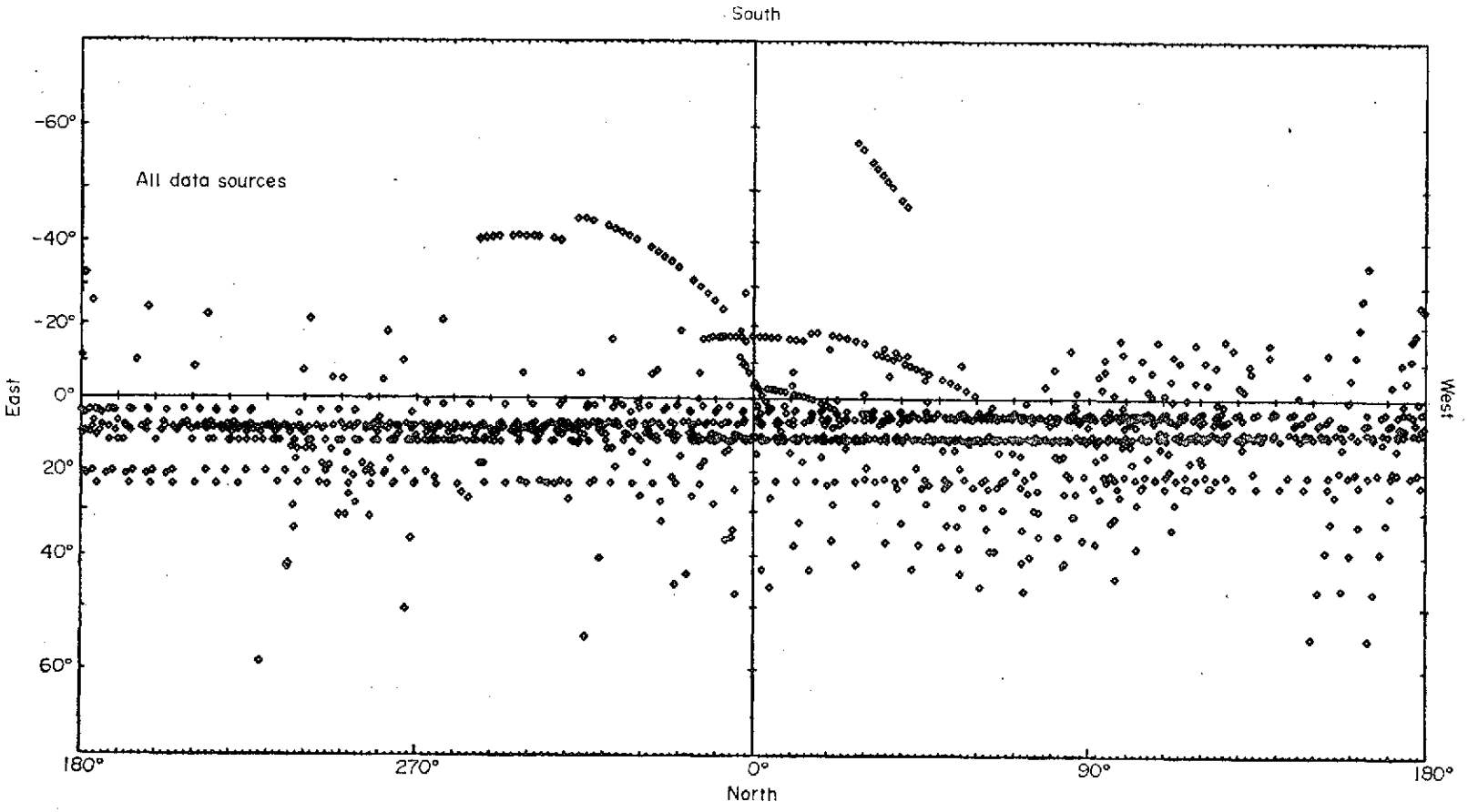

FIG. 18. The distribution of all 1382 data points on Mars from the four sources described in this report, which were used in the various stages of smoothing. Refer to Fig. 20 for their location on Mars.

has been lost from the very edges of the individual data arrays since the smoothing program rejected any values for a grid interval for which there were less than three points within the range of the resolution element. Most of those points affected in the Southern Hemisphere may become useable when ground-based CO_2 data from the current 1971 opposition is made available.

The final contour map is given in Figs 19 and 20. The first shows only the contours as in the other maps of this report. Fig. 20, however, shows the plot overprinted on a current map of Mars so that relationships with surface markings can be seen.

Associated with these contours, the corresponding smoothing errors are given in Fig. 21. The range of $\bar{s}$ is from 0·1 to 2·9 km in 0·2 km steps. The largest errors again are associated with the apparent topographic slopes at 260°, 60°, 150° and 170° W. The most reliable portions of the topographic map are represented by blank regions in the contoured areas of Fig. 21. These correspond to errors in the combination of less than 0·5 km. Fig. 21 indicates at a glance those areas which should be regarded only with extreme caution as being real. Most of these areas are located at the edges of the mapped areas.

7. Discussion

A point of interest in Fig. 20 is an attempt to establish any relationship between the distributions of surface markings and those of altitudes and slopes. This examination can be done in a quantitative manner by statistics, but will be deferred to Part II of this report in which the 5°-grid data will be regenerated on a 1°-grid interval by spherical harmonics. Nevertheless, a visual inspection of Fig. 20 shows some results that can be expected from a more detailed analysis.

In general, no relationship is apparent between topographic heights and the distribution of dark areas on the planet. Some dark areas are apparently situated on parts of measured slopes: Cerberus (200° W, 10° N), Syrtis Major (290° W, 10° N), Hellespontus (320° W, −50° S), Sinus Meridianii (0°, 0°), Margaritifer Sinus (20° W, −10° S), and Mare Acidalium (30° W, 35°N). This apparent correlation may have no significance when one considers that practically all bright desert areas thus far measured are also associated with slopes. The highest areas on Mars, so far, are seen to be deserts (Tempe [65° W, 50° N] at +12 km; and Tharsis [110° W, 10° N] at +7 km), but the lowest areas are also deserts (Hellas [300° W, −50° S] at −2 km; Chryse-Xanthe [30° W, 10° N] at −2 km; and Memnonia [160° W, −20° S] at −6 km).

It should be noted that the base map of Fig. 20 is the recent one published by the Lowell Observatory made from ground-based photographs of Mars during the 1969 apparition. The co-ordinates of features were measured directly from these photographs. The positions in longitude correspond closely to those determined from the Mariner 6 and 7 photographs. However, for high southerly latitudes the agreement with the Mariner co-ordinates is not so good. This fact is due to the 1969 axial tilt of Mars which positioned the Martian south pole away from the Earth and to the fact that the south polar cap extended down to about −60° S.

The discrepancy is most pronounced in a comparison of the position of Hellas on the Lowell map (Lowell Observatory 1971) and on the NASA Mariner chart (U.S. Army Topographic Command 1970). The former places the southern limit of Hellas at about −60° S, while the Mariner map places this limit at about −55° S. The northern extent of the Hellas circle is put at −40° S on the Lowell map, while it is located at about −25° S on the Mariner map. The negative contours in the Hellas area fall more closely in the circular outline of Hellas on the Mariner chart than is evident in Fig. 20.

The Lowell map was used for the base map since the standard shapes of the dark markings drawn by air brush can be easily seen, whereas in the Mariner chart a large

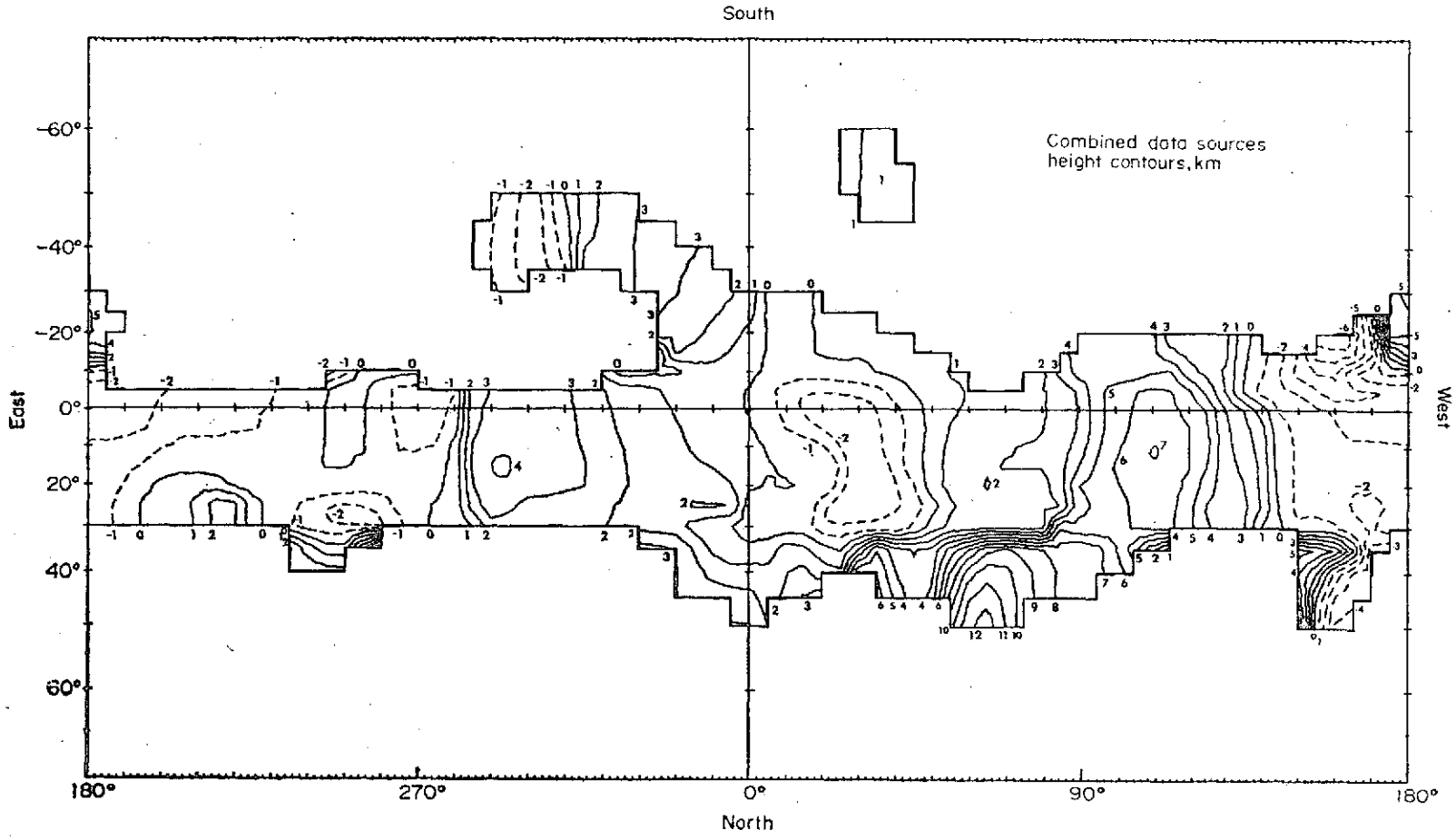

FIG. 19. The final height contour map resulting from the combination of the smoothed data of each of the four sources described in this report. The smoothed 5°-grid data of each source were simultaneously processed by equation (1) generating a 5° regular array of 924 values. As before, solid lines represent zero and positive topography, while dashed lines correspond to negative topography. The range of elevations is from −6 to +12 km in 1-km intervals. Features to be regarded with caution are those with steep slopes near the edges of the mapped areas and features smaller than the resolution element, see Fig. 21.

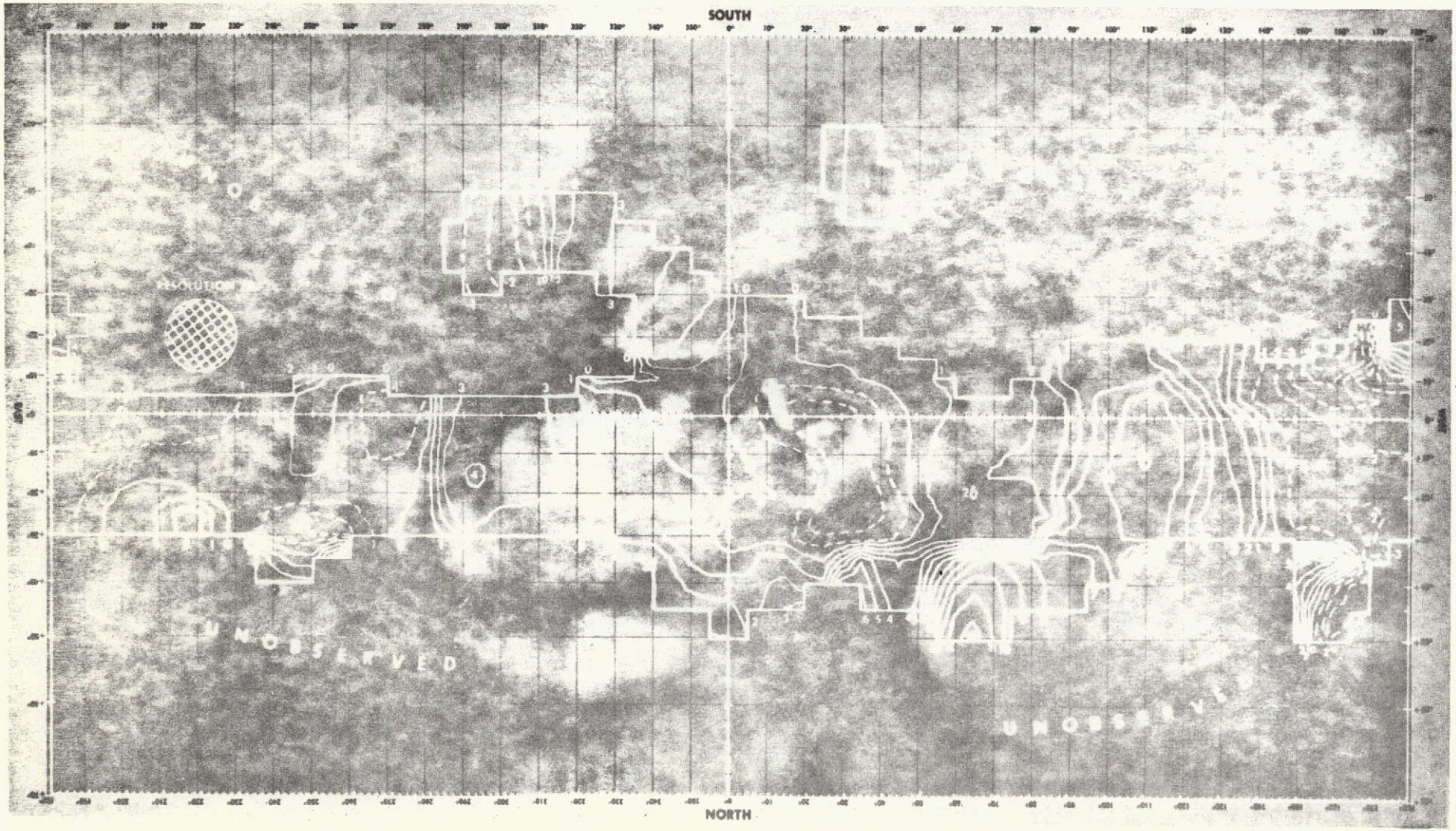

FIG. 20. Final height contours produced from the combined data sources listed in this paper superimposed on a map of Mars. The resolution element of 1000 km is shown by the cross-hatched circle to the left. The base map is that published by the Lowell Observatory in 1971 from the 1969 Mars Earth-based photographic patrol.

facing p. 130

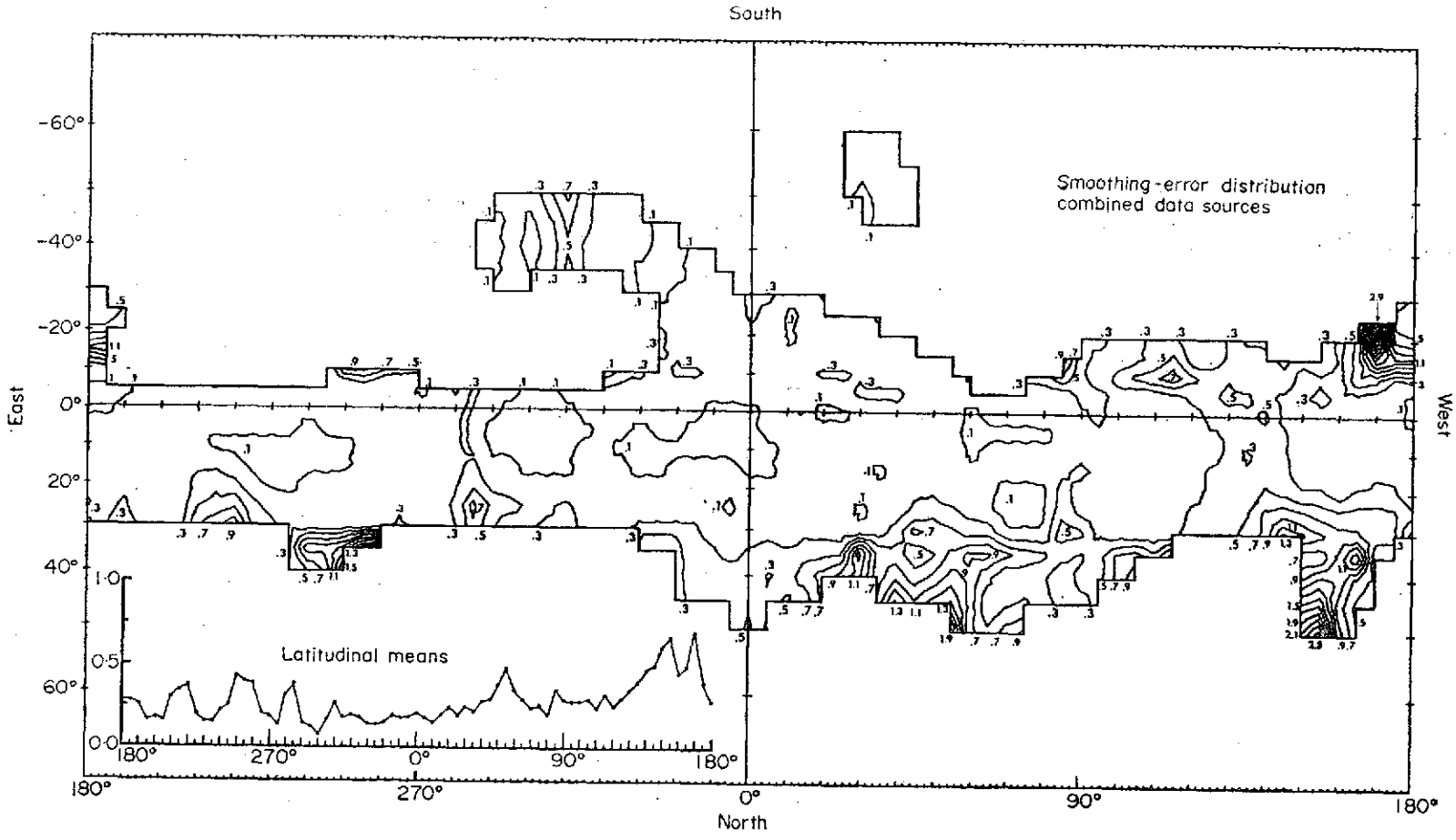

FIG. 21. Contours of the internal smoothing errors $\bar{s}$ derived from equations (2) for the final combination of the four smoothed data sources. Errors range from 0·1 to 2·9 km in 0·2 km intervals. Mean values of $\bar{s}$ with longitude are given in the lower left diagram. Areas of greatest suspicion are those where the contour lines crowd together, generally near the edges of the map boundaries. The largest portion of the map, however, is associated with smoothing errors smaller than 0·5 km.

section of the central area of the map contains airbrush inserts of the Mariner 6 and 7 near-encounter photographs making it difficult to follow the outlines of Sabaeus Sinus, Sinus Meridianii, Margaritifer Sinus, etc.

The position of the contours of Fig. 19 with respect to the surface markings therefore depends upon which chart is used for the base map. The analysis of surface altitudes and slopes vs. albedo, presented in Part II, will rely on the Mariner control net for co-ordinates.

Also of interest from Fig. 20 is the distribution of blocks and basins. The major high and low areas are two blocks and two basins centred approximately at 300° W (Syrtis Major), 30° W (Chryse-Xanthe), 110° W (Tharsis), and 180° W (Memnonia-Amazonis). They are spaced about 90° apart in longitude and together with their near equatorial position suggest the presence of a strong second harmonic. Other block- and basin-type features are apparent on the map as was mentioned at the beginning of this section. The precise harmonic distribution of these features will be found in Part II.

The term 'block' and 'basin' is used in a general sense by the writer since the geological terms 'ridge' and 'valley' convey a more specific meaning applicable to considerably smaller scaled features than are found in Fig. 20. It is possible that these blocks and basins could be structurally similar to the Earth's continents and ocean basins during primitive stages of the latter's formation. It is significant that on the scale of Mars, these features are much larger and higher than the corresponding structures on the Earth.

It has also not escaped the author's notice that the presence of large-scaled blocks and basins on Mars may have important geophysical consequences regarding the theory of continental drift and sea floor spreading as was suggested earlier (Wells 1969b, 1971).

Acknowledgments

The author thanks M. J. S. Belton and D. M. Hunten for independent participation in the Kitt Peak CO_2 experiment and in data reductions of the observations as well as provision of their measurements; G. H. Pettengill and A. E. E. Rogers for provision of the Haystack radar data in advance of publication; R. S. Goldstein for provision of the unpublished Goldstone radar data in tabular form; K. C. Herr for access to the Mariner IRS CO_2 data during various stages of preparation; and C. W. Hord for a copy of the Mariner UV surface altitude variations in graphical form. Computations were carried out on the Space Science Laboratory SDS Sigma 7 computer and the University of California Computer Center CDC 6400. Thanks are also due to M. J. S. Belton for provision of the contouring algorithms which were modified and adapted for the SSL SDS Sigma 7. This research was supported by NASA grant NGR 05-003-431.

Space Sciences Laboratory,
University of California,
Berkeley, 94720, U.S.A.

References

Barth, C. A. & Hord, C. W., 1971. *Science*, **173**, 197.
Belton, M. J. S. & Hunten, D. M., 1966. *Astrophys. J.*, **145**, 454.
Belton, M. J. S. & Hunten, D. M., 1969. *Science*, **166**, 225.
Belton, M. J. S. & Hunten, D. M., 1971. *Icarus*, **15**, 204.
Belton, M. J. S., Broadfoot, A. L. & Hunten D. M., 1968. *J. geophys. Res.*, 73, 4795.

Goldstein, R. M., Melbourne, W. G., Morris, G. A., Downs, G. S. & O'Handley, D. A., 1970. *Radio Science*, **5**, 475.

Herr, K. C., Horn, D., McAfee, J. M. & Pimentel, G. C., 1970. *Astr. J.*, **75**, 883.

Leovy, C. & Mintz, Y. A., 1969. *J. atmos. Sci.*, **26**, 1167.

Pettengill, G. H., Counselman, C. C., Rainville, L. P. & Shapiro, I. I., 1969, *Astr. J.*, **74**, 461.

Rogers, A. E. E., Ash, M. E., Counselman, C. C., Shapiro, I. I. & Pettengill, G. H., 1970. *Radio Science*, **5**, 465; also ' Radar Studies of Mars ', report under contract NAS 9–7830, Lincoln Laboratory, Mass. Inst. of Tech., 15 Jan. 1970.

Wells, R. A., 1969a. *Science*, **166**, 862.

Wells, R. A., 1969b, *Geophys. J. R. astr. Soc.*, **18**, 109.

Wells, R. A., 1971. *Phys. Earth Planet. Int.*, **4**, 273, special issue, NATO Advanced Studies Institute, Newcastle upon Tyne (April 1970).

Relief-Darstellung der Marsoberfläche

■ *Radarabtastung / Infrarot-Spektroskopie / Oberflächenmodell / Kontinentaldrift?*

Die ausgezeichneten Photographien, welche von den Marssonden Mariner IV, VI, VII und IX zur Erde zurückgefunkt wurden, haben eine Fülle neuer und überraschender Erkenntnisse über unseren äußeren Nachbarplaneten geliefert. Allerdings war es an Hand dieser Aufnahmen noch nicht möglich, die Höhen- und Tiefenlage eines größeren Gebietes kartenmäßig zu erfassen. Dies gelang erst, als man die weiteren Beobachtungstechniken der Radarabtastung und Infrarot-Spektroskopie heranzog. Mit Hilfe dieser Methoden hat man neue Einsichten in die geophysikalische Geschichte der Oberfläche des Mars erhalten, eines Planeten, der topographische Unterschiede im Großen besitzt, die den Kontinenten und Ozeanbecken der Erde vergleichbar sind.

Aus den Mars-Photographien, die von den vier amerikanischen Mariner-Raumschiffen 1965, 1969 und 1971–72 aufgenommen wurden, war zu ersehen, daß die Marsoberfläche sehr unterschiedliche Strukturen aufweist: Kraterlandschaften, Gebiete ohne Kraterspuren, unregelmäßig strukturierte Gelände und weit ausgedehnte, stark verworfene Zonen [1]; (vgl. auch UMSCHAU 1972, Heft 4, S. 119, Heft 7, S. 206; 1969, Heft 19, S. 616).

Die Photos enthalten beispielsweise Kraterwände, Grate und Verwerfungen mit einer Ausdehnung von kleiner als ungefähr 100 km. Die senkrechten Höhen lassen sich mit Hilfe der Schatten- und Albedomessungen bestimmen. Dagegen sind die Höhenlagen der flächenhaften Ausdehnungen mit Durchmessern größer als etwa 1000 km nicht meßbar, da die Schatten dieser Objekte nicht auswertbar sind. Das Stereomeßbildverfahren ist wegen des großen Abstandes der Sondenkamera von der Marsoberfläche zur Höhenbestimmung noch nicht geeignet.

Oberflächenstrukturen großer Ausdehnung konnten dagegen durch Radarabtastung von der Erde aus vermessen werden [2], wobei die jeweiligen Höhenlagen sich als Zeitverspätungen der Radarechos bemerkbar machten. Obgleich der auftreffende Radarstrahl die gesamte Marsscheibe überdeckt, kommt das für die Höhenbestimmung benutzte reflektierte Signal nur vom erdnächsten Punkt der Marsoberfläche. Das begrenzte Auflösungsvermögen des Radarteleskops verursacht eine Unschärfe dieser Stelle von ungefähr 300 km. Die unterschiedliche Richtung der Rotationsachse des Mars relativ zur Beobachtungsstation ermöglichte die Vermessung der Gebiete zwischen 0° und 20° nördlicher Breite während der beiden Beobachtungszeiten in den Jahren 1967 und 1969.

Eine zweite Methode benutzt die Infrarotabsorption in einem CO_2-Band bei einer Wellenlänge von 1,05 μm [3]. Da die Marsatmosphäre hauptsächlich aus CO_2 besteht, ergibt diese Messung den CO_2-Gehalt in einer senkrechten Säule über einem bestimmten Gebiet auf der Marsoberfläche. Die CO_2-Konzentration ergibt den Druck am tiefsten Punkt der Atmosphäre, woraus sich die jeweiligen Oberflächenhöhen durch die isothermische barometrische Gleichung errechnen lassen. Weil das optische Fernrohr auf jede Stelle der Marsoberfläche gerichtet werden kann, gibt es keine von der Marsachse beeinflußten Breitengrenzen wie bei der Beobachtung mit einem Radarteleskop. So kann man während einer Marsopposition mit der spektroskopischen Methode beträchtlich mehr Daten als mit der Radarabtastung erhalten. Die spektroskopischen Beobachtungen wurden in dem Kitt Peak National Observatory in Tucson (Arizona) während des Sommers 1969 mit einem Sonnenteleskop gewonnen.

Die dritte Technik ist ebenfalls spektroskopischer Art: das Infrarotspektrometer befindet sich jedoch in einem Raumschiff [4]. Die

Bild 1: Höhenlinienkarte der Marsoberfläche, die auf Grund der Radar- und CO_2-Messungen konstruiert wurde. Die Höhenlinienabstände betragen 1 km. Die Höhen erstrecken sich von −6 km bis zu +12 km. Die Nullhöhe in einer isothermischen Atmosphäre gleicht 5,5 mb CO_2, die auch dem Marsradius 3393 km entspricht. Die dicken Linien bezeichnen positive Höhen, die gestrichelten Linien negative Höhen. Der kreuzschraffierte Kreis bei der Länge 220° kennzeichnet das Auflösungsvermögen der zusammengefaßten Daten und hat einen Durchmesser von etwa 1000 km.

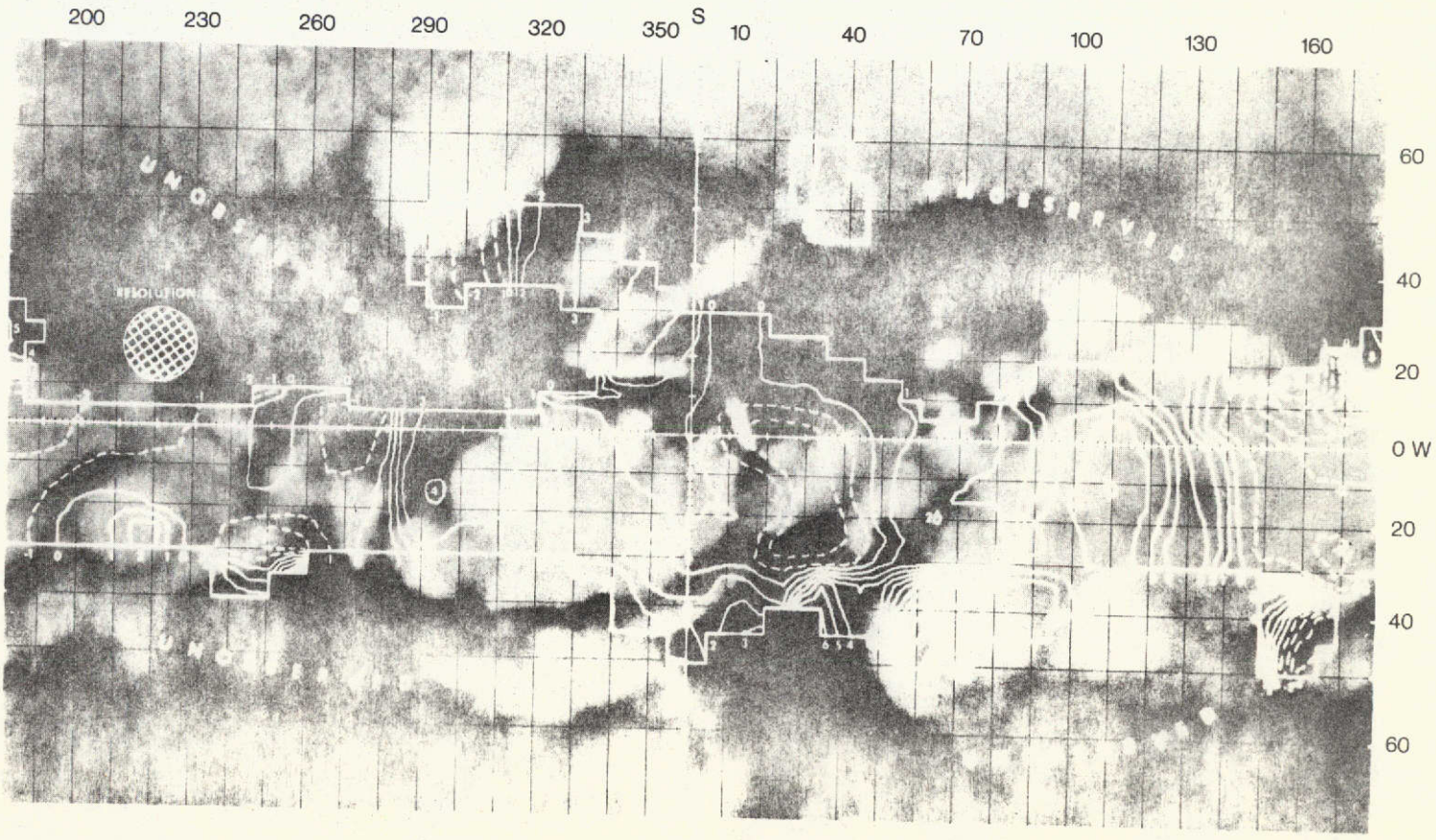

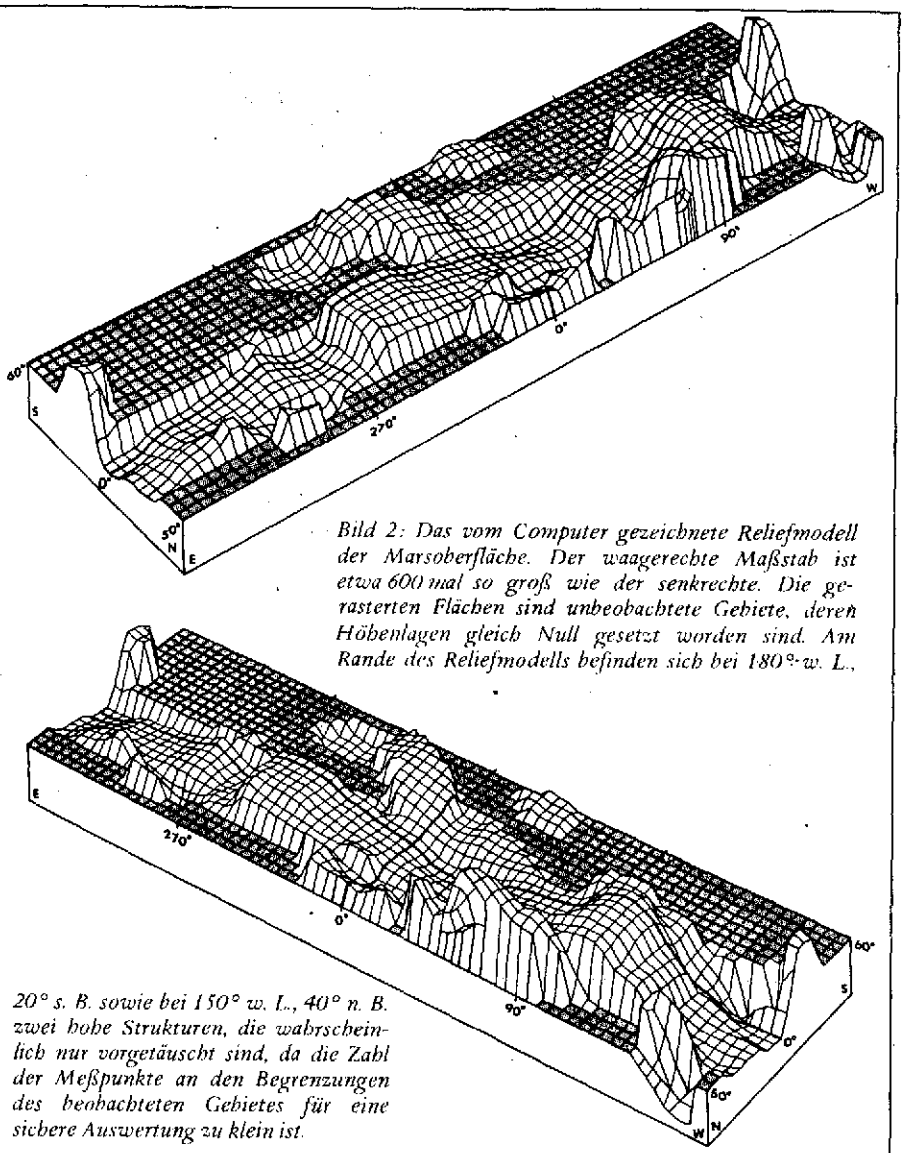

Bild 2: Das vom Computer gezeichnete Reliefmodell der Marsoberfläche. Der waagerechte Maßstab ist etwa 600 mal so groß wie der senkrechte. Die gerasterten Flächen sind unbeobachtete Gebiete, deren Höhenlagen gleich Null gesetzt worden sind. Am Rande des Reliefmodells befinden sich bei 180° w. L., 20° s. B. sowie bei 150° w. L., 40° n. B. zwei hohe Strukturen, die wahrscheinlich nur vorgetäuscht sind, da die Zahl der Meßpunkte an den Begrenzungen des beobachteten Gebietes für eine sichere Auswertung zu klein ist.

fehlenden Störeinflüsse der Erdatmosphäre erlauben eine erheblich größere Auflösung der Beobachtungsobjekte. Nachteilig ist allerdings, daß nur ein begrenzter Streifen der Marsoberfläche in einem einzigen Vorbeiflug beobachtet werden kann. Wegen der Marsrotation wird aber von der Satellitensonde im Verlauf einiger Tage fast jeder Punkt der Oberfläche überflogen. Die neuesten Messungen von Mariner IX sind leider durch Staubstürme stark beeinträchtigt.

Die drei Untersuchungsmethoden ergeben Daten mit verschiedener Auflösung. Die Mariner VI- und VII-Daten erreichen eine Oberflächenauflösung von 130 × 8 km². Die Auflösung der Radarergebnisse entspricht einem Kreis von etwa 300 km Durchmesser und die CO_2-Messungen von der Erde einem Quadrat von etwa 1000 km Seitenlänge. Um eine gute übersichtliche Darstellung zu erhalten, werden zweckmäßigerweise die Daten aus allen drei Beobachtungsverfahren in einem Modell berücksichtigt. Die Datenverteilung hat es erlaubt, das Vereinigungsverfahren in 5°-Abständen durchzuführen, wodurch dann aber die Meßpunkte die geringste Auflösung (1000 km) haben.

Mit den gewonnenen Daten ist eine Höhenlinienkarte der Oberfläche *(Bild 1)* vom Computer gezeichnet worden. Dieselben Ergebnisse sind in Form eines Reliefmodells, das ebenfalls von einem Computer erstellt worden ist, dargestellt worden *(Bild 2)*. Auf der Höhenlinienkarte sehen wir, daß die größten Höhenunterschiede auf dem Mars etwa 18 km betragen, wenn wir den Gebirgsblock (+12 km) bei 65° und das Becken (−6 km) bei 160° westlicher Länge betrachten. Diese Kontinente zwischen 90° und 130° bzw. zwischen 280° und 320° sind beide fast so groß wie Australien. Das Becken zwischen etwa 150° und 180° ist größer als das Mittelmeer, und das große Zentralbecken bei 30° ist breiter als der Atlantische Ozean.

Aus der Oberflächenform ist ferner die sogenannte Oberflächen-Harmonik berechnet worden, ein mathematischer Ausdruck, der die Abweichungen der wirklichen Marsoberfläche von der einer Kugel beschreibt. Aus den harmonischen Koeffizienten ist schließlich das Gravitationsfeld des Planeten berechnet worden. Eine sehr genaue Bestimmung (einschließlich Glieder 6. Ordnung) des Mars-Gravitationsfeldes ist kürzlich auf Grund der Bahnstörungen von Mariner IX vorgenommen worden. Den Forschern gelang es, aus den Werten für das Gravitationsfeld die entsprechenden Oberflächenhöhen zu errechnen. Somit ist es nun möglich, die Ergebnisse der Höhenmessungen miteinander zu vergleichen. *Bild 3* zeigt die vorläufigen Werte der Oberflächenhöhen für die verschiedenen Meßmethoden. Die Kurven repräsentieren Profile, die aus *Bild 1* und der in [5] publizierten Höhenlinienkarte entnommen wurden. Sie folgen den Breitenkreisen auf 5° nördlicher und 15° südlicher Breite. Die Übereinstimmung hinsichtlich der Richtung der Höhenveränderungen von den Kurven ist recht gut. Eine Korrelationsrechnung, die auf wachsenden Höhenwerten basiert *(Bild 3*, oben), liefert einen Korrelationskoeffizienten von 70%.

Aus *Bild 1* kann gefolgert werden, daß keinerlei Zusammenhang zwischen der Albedo und der Höhe der Oberfläche besteht. Es gab Kontroversen über die Morphologie der dunklen Oberflächengebiete des Mars [6], die man wie beim Mond „Maria" nennt. Es ging um die Frage, ob die dunklen Gebiete Hoch- oder Tiefländer sind. Wie man aus *Bild 1* ersehen kann, können die dunklen Gebiete sowohl hoch als auch tief liegen, genau so wie die hellen Gebiete, die meist als „Wüsten" bezeichnet werden. Dieses Ergebnis ist ein Hinweis darauf, daß die unterschiedliche Helligkeit der Gebiete durch die Verschiedenheit der chemischen Zusammensetzung der Oberflächen hervorgerufen wird.

Besonderes Interesse gilt den großen Landmassen, den „Urkontinenten". Mit Ausnahme der Erde und jetzt des Mars sind bisher keine Kontinente auf anderen Planeten sicher festgestellt worden. Es wäre denkbar, daß auf dem Mars, wie bei der Erde, eine Kontinentaldrift und Ausbreitung des Meeresbodens stattfindet. Daher wird der Mars für Geophysiker eine neue und wichtige Rolle spielen. Im Zusammenhang mit diesen Prozessen weisen theoretische Berechnungen darauf hin, daß die Konvektion innerhalb des äußeren Marsmantel die treibende Kraft für große Krustenbewegungen sein kann [7].

Ein Vergleich der Photographien des kraterförmigen Terrains mit den Ergebnissen der Radar- und Infrarotmessungen ergibt, daß der Mars eine Oberflächenstruktur hat, die teilweise große Ähnlichkeit mit der des Mondes besitzt, aber auch an die Kontinente der Erdoberfläche erinnert.

Die hier beschriebenen Untersuchungen wurden von NASA Grant NGR 05-003-431 gefördert. Der Autor dankt Dres. *J.-P. Pfeifer* und *B. Simoneit* für die Hilfe bei der Übertragung des Textes ins Deutsche.

Wells, R. A.: Relief-Darstellung der Marsoberfläche. UMSCHAU 72 (1972) Heft 9, S. 293–295.

Summary:

The Mariner 4, 6, 7 and 9 spacecraft have returned many excellent photographs of the surface of Mars; however, it has not been possible to obtain information from them concerning the relief of large-scale surface features. Altitude information of the grosser features of the surface has been derived

from the two techniques: direct radar-ranging from the Earth, and infrared CO_2 spectroscopy of the Martian atmosphere using both Earth-based and onboard spacecraft spectrometers. These data have been combined into a homogeneous array of surface heights which has been contoured by a computer. The resulting topographic contour map shows the presence on Mars of block and basin features that are comparable in areal extent to the continents and ocean basins of the Earth.

Literatur:

[1] Mariner 6 and 7 Summary of Results. J. Geophys. Res. *76* (1971) S. 293–444; Mariner 9 Television Reconnaissance of Mars and Its Satellites: Preliminary Results. Science *175* (1972) S. 294–305.

[2] *Rogers, A. E. E.; Ash, M. E.; Counselman, C. C.; Shapiro, I. I.; Pettengill, G. H.:* Radio Science *5* (1970) S. 465.

[3] *Wells, R. A.:* Science *166* (1969) S. 862; Analysis of Large-Scale Martian Topography Variations. Geophys. J. Roy. Astron. Soc (1972) in press.

[4] *Herr, K. C.; Horn, D.; McAfee, J. M.; Pimentel, G. C.:* Astron. J. *75* (1970) S. 883.

[5] *Lorell, J.; Born, G. H.; Christensen, E. J.; Jordan, J. F.; Laing, P. A.; Martin, W. L.; Sjogren, W. L.; Shapiro, I. I.; Reasenberg, R. D.; Slater, G. L.:* Science *175* (1972) S. 317.

[6] *Wells, R. A.:* Geophys. J. Roy. Astron. Soc. *17* (1969) S. 209; Ibid. *18* (1969) S. 109.

[7] *Schubert, G. C.; Turcotte, D. L.; Oxburgh, E. R.:* Geophys. J. Roy. Astron. Soc. *18* (1969) S. 441.

Dr. *R. A. Wells,*
Space Sciences Laboratory,
University of California,
Berkeley, Calif., USA

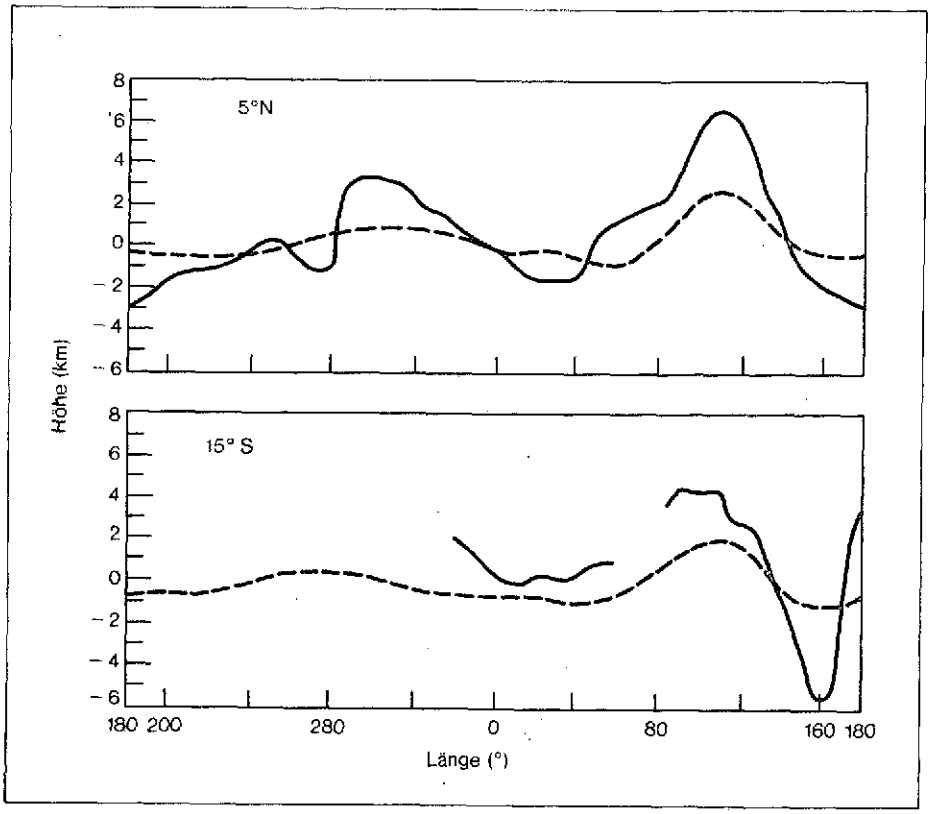

Bild 3: Ein Vergleich der Höhenbestimmungen der Marsoberfläche nach verschiedenen Methoden. Die ausgezogene Kurve zeigt die direkten Höhenmessungen der Radar- und Infrarotbeobachtungen. Die gestrichelte Linie repräsentiert die Oberflächenhöhen, die aus der Analyse der Bahnstörungen der Marssonde Mariner IX errechnet wurden. Das Höhenprofil oben bzw. unten verläuft entlang 5° nördlicher bzw. 15° südlicher Breite.

АКАДЕМИЯ НАУК СССР

АСТРОНОМИЧЕСКИЙ ЖУРНАЛ

Том 49

(ОТДЕЛЬНЫЙ ОТТИСК)

3

МОСКВА · 1972

АСТРОНОМИЧЕСКИЙ ЖУРНАЛ

Том 49 1972 Вып. 1

УДК 523.43

Р. А. УЭЛЛЗ

ТОПОГРАФИЯ МАРСА ПО ДАННЫМ НАЗЕМНЫХ РАДИОЛОКАЦИОННЫХ ИЗМЕРЕНИЙ И ПО НАБЛЮДАЕМОМУ С ЗЕМЛИ И С КОСМИЧЕСКИХ АППАРАТОВ «МАРИНЕР-6 И 7» ПОГЛОЩЕНИЮ CO_2

Совместно анализируются все известные к настоящему времени данные о вариациях высот (топографии) Марса, осредненные на одинаковых интервалах разрешения. Установлено, что суммарная разность высот на Марсе достигает почти 18 *км*, что соответствует изменениям давления (CO_2) с 2 *мб* на высоте 12 *км* до 10 *мб* на уровне 6 *км*.

MARTIAN TOPOGRAPHY FROM EARTH-BASED RADAR, EARTH-BASED CO_2, AND THE MARINER 6 AND 7 CO_2 MEASUREMENTS, by *R. A. Wells*.— All presently available data sources of martian topographical variations have been combined and smoothed to the same spatial resolution limit. The total height range on Mars is found to be nearly 18 *km* corresponding to a CO_2 pressure range from 2 *Mb* at 12 *km* to 10 *Mb* at — 6 *km*.

Данные о топографии отдельных областей на Марсе быстро накапливались в течение прошедших трех лет. Эта проблема прежде была предметом достаточно произвольных предположений [1]. В настоящее время морфология поверхности Марса в масштабе порядка 1000 *км* может изучаться с использованием точной техники радиолокационного зондирования и спектроскопических определений содержания CO_2 в атмосфере планеты.

При составлении марсианской топографической карты использовались материалы, которые позволили произвести первое определение разностей высот по радиолокационным отражениям (высоты поверхностей измеряются по отставанию возвращающихся эхо), эти материалы получены Петтенгилом и др. в 1967 г. [2], Роджерсом и др. в 1969 г. [3], Голдстейном и др. в 1969 г. [4], кроме того, использовались результаты определений содержания CO_2, полученных Белтоном и Хантеном [5] и Уэллсом [6] в 1969 г., а также определения количества CO_2 по данным инфракрасных спектрометров «Маринера-6 и 7» в 1969 г. [7].

Результаты Барта и Хорда [8], основанные на данных спектроскопии в ультрафиолетовой области, не учитывались непосредственно при расчетах из-за неопределенности допущений в применявшейся ими модели атмосферы. Однако эти результаты использовались для сравнения с инфракрасными спектрами, так как обоими инструментами изучались примерно одни и те же области планеты.

Составление новой и более точной карты рельефа наблюдаемых областей Марса является основной целью настоящей статьи. В сущности карта представляет собой промежуточную ступень в более детальном гармоническом анализе поверхности, который автор надеется опубликовать в недалеком будущем.

Данные оригинальных источников распределены весьма неравномерно в пределах площади планеты, ограниченной примерно 50° северной и 20°

южной широты (за исключением области, охваченной измерениями «Маринера-7», которая пересекает детали Noachis — Hellespontus — Hellas) по всей долготе. Для использования в гармоническом анализе необходимо перевести данные в прямоугольную систему координат и пересчитать их к одному и тому же масштабу сечения, например к наименьшему сечению. Радарные измерения покрывают площадь круга диаметром 300 *км*, измерения содержания CO_2 с Земли соответствуют квадрату со стороной 1000 *км*, а данные «Маринера» — прямоугольнику размером 130·8 *км*.

Перевод данных в прямоугольную систему координат и снижение пределов разрешения к наиболее низкому из имеющихся ($\approx$1000 *км* или 18° поверхности) может быть выполнено одновременно при помощи функции кругового распределения Гаусса:

$$\bar{Z} = \frac{\sum_i z_i e^{-r_i^2/2\sigma^2} \rho_i^{-2}}{\sum_i e^{-r_i^2/2\sigma^2} \rho_i^{-2}}, \qquad (1)$$

где средневзвешенная высота $\bar{Z}$ определяется из совокупности отдельных частных высот z_i в пределах радиуса 9° от пересечения координат; r_i — расстояния до каждой из i-х точек от пересечения координат, вычисленные посредством сферической тригонометрии; σ — полуширина трехмерной огибающей Гаусса, в данном случае выбранная так, чтобы радиус разрешения в пределах 9° составлял $1/e$; ρ_i — стандартное отклонение для каждой из высот. В случае использования атмосферной техники с привлечением данных CO_2 слектроскопии в уравнение (1) вводится взвешенная функция, эквивалентная обратному натуральному логарифму воздушной массы для каждой из высот z_i. Воздушная масса служит фактором для определения давления (чем меньше воздушная масса, тем точнее вычисляемое давление), а давление и высота связаны логарифмически.

Определения содержания CO_2 с Земли [5, 6] были закончены летом 1970 г. в национальной обсерватории Китт Пик. Редукции включают точные связи кривых роста CO_2 и поправки на дифференциальную рефракцию и дисперсию. Детальные расчеты этого анализа содержатся в [9].

Дифференциальная рефракция, дисперсия и преломление световых лучей, проходящих через атмосферу Земли, приводят к значительному смещению точек наблюдений, что в итоге сводится к сгущению точек на поверхности Марса к северу и востоку.

При совместном анализе данных интерес представляет сравнение высот, полученных методом радиолокационного зондирования и посредством определения содержания CO_2. Нулевой уровень по радиолокационным данным отнесен к геометрическому центру планеты, тогда как для CO_2 нулевой уровень соответствует центру тяжести. В случае несовпадения обоих центров возможна разница в нулевых уровнях.

При использовании данных измерений CO_2 с Земли точные значения высот могут быть найдены лишь в случае полного покрытия поверхности по долготе. Это обстоятельство вытекает из зависимости

$$\eta p_{CO_2} = Cf(\eta, p_{CO_2}, T)(\gamma S_0 - S_1), \qquad (2)$$

где η — воздушная масса; p_{CO_2} — давление CO_2; T — температура атмосферы; $f(\eta, p_{CO_2}, T)$ — функциональная связь, определяемая по кривой роста для CO_2; S_0 — интенсивность сигнала калибровки по вольфрамовой нити лампы; γS_0 — величина сигнала при регистрации спектра Луны, т. е. стандарт для случая нулевого поглощения; S — интенсивность линий в области 1.05 *мкм*; C — постоянная калибровки. Редукция данных зависит от величины C. Константа C позволяет связать каждое из ночных наблюдений,

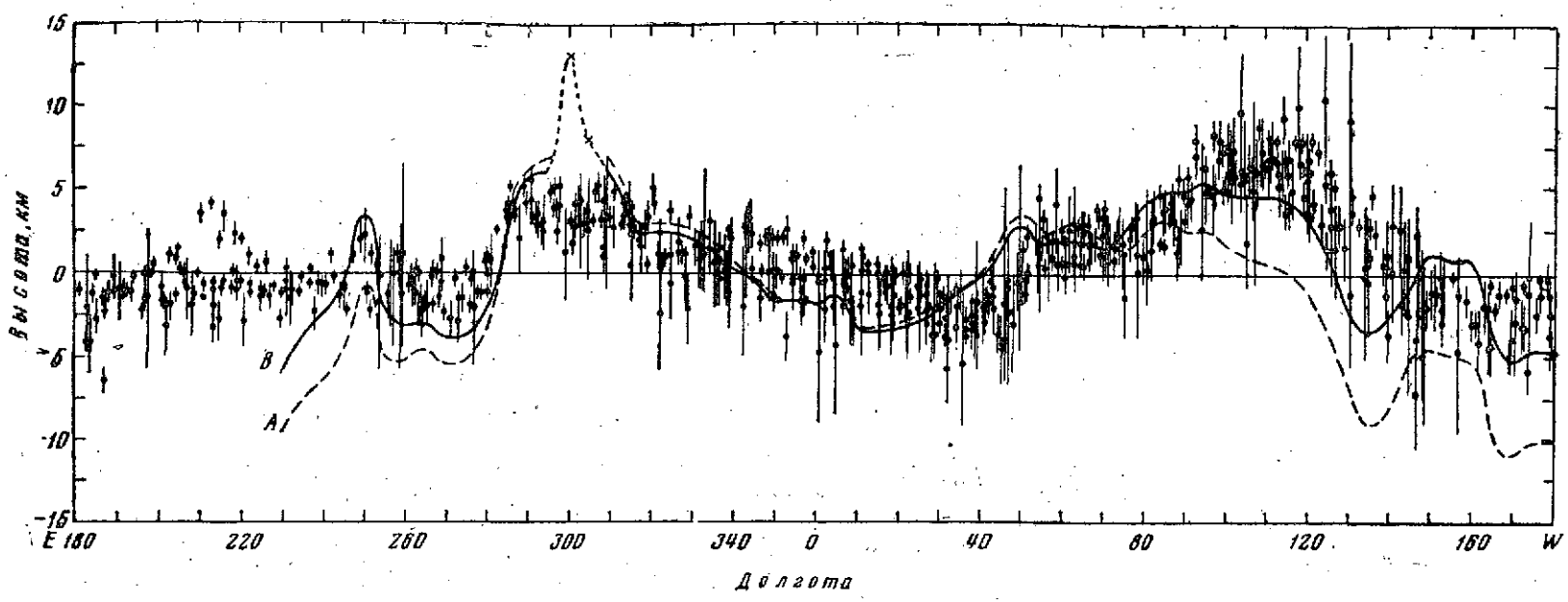

Рис. 1. Сравнение средних высот, определенных по CO_2 для интервала 0 и 21° N широты и разных долгот до нормализации (кривая *A*) и после нормализации (кривая *B*) с радарными данными (заполненные кружки) в пределах того же широтного интервала. Точки радарных данных имеют пределы ошибки в 1 стандартное отклонение и соответствуют оригинальному пространственному разрешению в 300 *км*. Данные по CO_2 были сглажены с разрешением в 1000 *км*. Расхождение (точечная линия) при длине 300° нельзя считать существенным из-за экспоненциальной потери чувствительности инструмента к высоте с ростом высоты. Эти CO_2-данные имеют очень незначительный удельный вес в сглаживающих расчетах

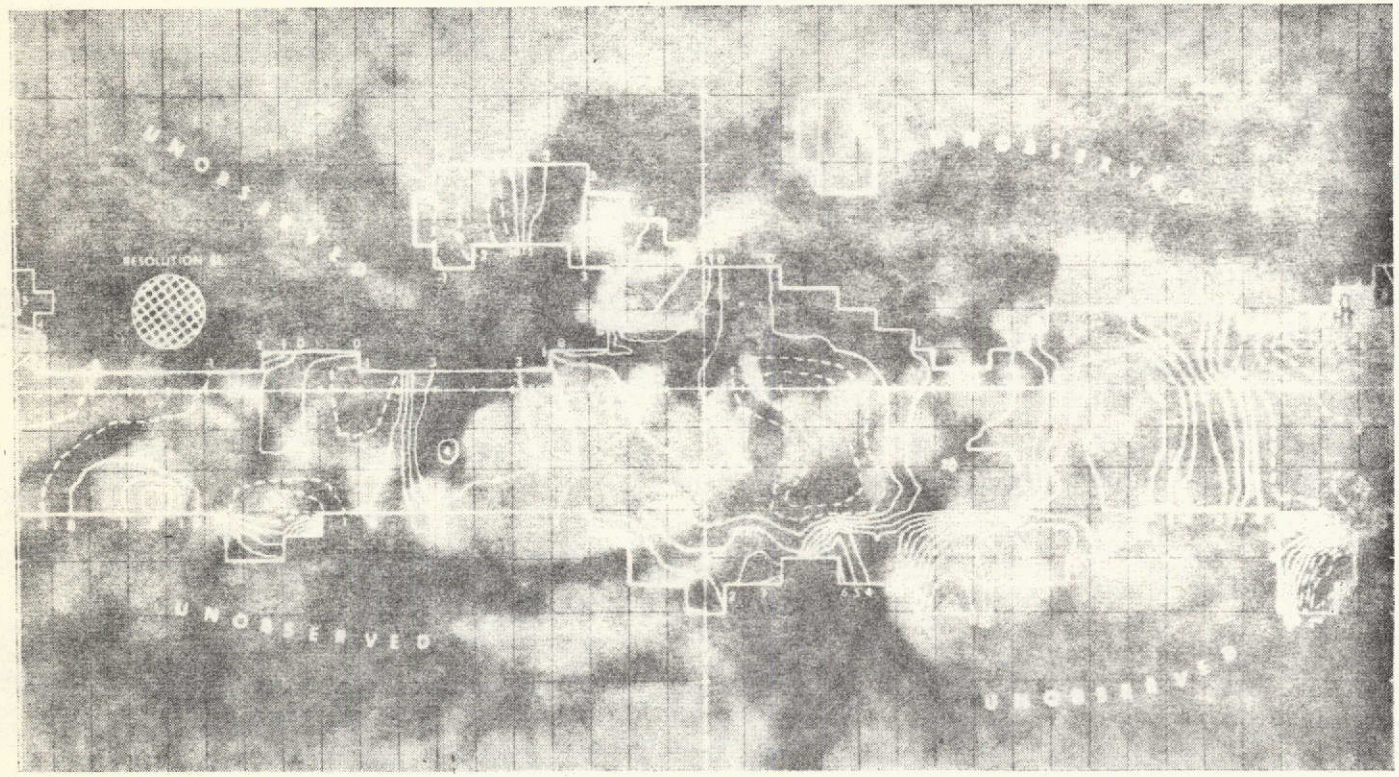

Рис. 2. Карта поверхности Марса в изолиниях по высотам, интерполированным на базе данных, выраженных на правильной сетке размеров 5° × 5°. Сплошные линии соответствуют положительным высотам, прерывистые — отрицательным высотам. Данные четырех источников, обсуждаемых в тексте, необходимых для составления этой карты, были объединены статистически. Заштрихованный круг слева соответствует приближенному размеру элемента разрешения. Особенности меньше, чем пределы разрешения, могут быть недействительными. Также с осторожностью следует относиться к элементам, соответствующим изолиниям на краях разверток в северной и южной полусферах

Рис. 3. Модель поверхности Марса, сделанная из папье-маше по данным рис. 2. Эта трехмерная модель обеспечивает большую наглядность изменений поверхности. В заштрихованной площади наблюдения отсутствуют

поскольку районы наблюдений перекрываются от ночи к ночи. Так как перекрытие по долготе не является полным, независимое абсолютное сравнение с наземными радиолокационными данными не представляется возможным. Однако авторы радиолокационных наблюдений не приводят сведений об измеряемом отклонении центра тяжести от геометрического центра Марса, поэтому мы вправе использовать радиолокационные данные в пределах 0—21° N широты для определения величины C в уравнении (2), при помощи которого можно было бы рассчитать абсолютную «спектроскопическую» высоту. В этом случае высоты, определенные по поглощению CO_2, точно нормированы к радиолокационным данным.

На рис. 1 изображены вариации содержания CO_2 над средней поверхностью в пределах 0—21° N широты в сравнении с оригинальными данными радиолокационных измерений [2, 3], относящихся к той же площади.

Данные по CO_2, полученные «Маринером-7», также были нормированы к радиолокационным измерениям [2, 3]. Это оказалось возможным благодаря двум перекрытиям полос «Маринера-6 и -7» с радиолокационными развертками.

Радиолокационные данные, полученные Голдстейном и др. [4], довольно удовлетворительно согласуются с данными Петтенгила и др. [2] и Роджерса и др. [3]; однако небольшая положительная коррекция порядка 0.7 *км* данных Голдстейна существенно улучшает дополнительно отмеченное согласование.

Перед сглаживанием с использованием уравнения (1) все имеющиеся в нашем распоряжении результаты были приведены к радиолокационному нулевому уровню. Данные всех четырех групп были затем объединены с помощью уравнения (1). Результат показан на рис. 2. Сплошными изолиниями изображены возвышения, прерывистыми — впадины. Наиболее приподняты участки планеты в пределах Tharsis и Tempe — от 7 до 12 *км*. Наиболее опущенный участок расположен в Memnonia — около —6 *км*. Суммарный перепад высот равняется 18 *км* и соответствует изменению давления чистой CO_2 от ~ 2 *мб* до ~ 10 *мб*.

На рис. 3 показана модель поверхности, изготовленная из папье-маше, по данным рис. 2. Перепады высот на этой трехмерной модели более наглядны.

Представляет интерес сравнение карты с точками касания сигналов с «Маринеров». Из шести точек с «Маринеров -4, -6 и -7» только одна попадает непосредственно в пределы карты. Это точка входа в радиотень «Маринера-6» с координатами 3.7° N; 4.3° W; давление в этой точке 5.5 ± 0.5 *мб* [10]. Оно соответствует высотному интервалу 0 ± 1 *км*; на карте точка расположена между изолиниями 0 и 1 *км*. Учитывая, что метод касательных точек основывается на тангенциальном касании планетарного лимба, совпадение следует считать весьма удовлетворительным.

Детальный анализ склонов, корреляция высот и крутизны склонов с альбедо поверхности и данные гармонического анализа будут опубликованы позднее. Можно, однако, прийти к заключению, что, по-видимому, не существует связи между высотами и крутизной склонов, с одной стороны, и альбедо поверхности — с другой. Максимальный уклон (по всей вероятности, порядка 3°) характерен для восточной части Syrtis Major и около 1° для юго-западного склона возвышенности Tharsis и восточной части Hellas — Hellespontus. Наличие крупных блоков и бассейнов на Марсе, по-видимому, обязано эволюции внутренних частей планеты. Вместе со сделанными «Маринерами» фотографиями заполненной множеством кратеров поверхности этот факт свидетельствует о том, что Марс является гибридной планетой между Землей и Луной в геофизическом смысле эволюционных процессов.

Автор благодарит М. Дж С. Белтона и Д. М. Хантена за предоставленную возможность использовать их оборудование и за участие в окончательной обработке измерений CO_2 с Земли; Г. Х. Петтенгила и А. Е. Е. Роджерас за предоставленную неопубликованную информацию радиолокационных измерений 1967 и 1969 гг., Р. М. Голдстейн за радиолокационные данные 1969 г.; К. С. Херр и Г. С. Пиментел за согласие использовать данные икс «Маринеров-6 и 7» и С. А. Барт и С. У. Хорд за использованные УФ-спектры «Маринеров-6 и 7». Автор также благодарит В. Вычева за помощь при переводе статьи на русский язык.

Лаборатория космических исследований
Калифорнийский университет
Беркли, Калифорния 94720
США

Поступила в редакцию
1 июля 1971 г.

Литература

1. Г. Н. Каттерфельд, Изв. Всесоюзн. геогр. о-ва, 91, 272, 1959; D. G. Rea, Nature, **200**, 114, 1963; **201**, 1014, 1964; R. A. Wells, Nature, **207**, 735, 1965; **209**, 1338, 1966; C. W. Tombaugh, Nature, 209, 1338, 1966; S. Miyamoto, Icarus, 5, 360, 1966; A. Dauvillier, Ciel et Terre, **83**, 384, 1967; E. J. Öpik, Science, **155**, 355, 1967; R. A. Wells, G. Fielder, Science, **155**, 354, 1967; C. Sagan, J. B. Pollack, R. M. Goldstein, Astron. J., **72**, 20, 1967; R. A. Wells, Geophys. J. Roy. Astron. Soc., **17**, 209, 1969; **18**, 109, 1969. Ю. А. Ходак, Изв. АН СССР. Сер. геол., № 1, 31, 1969.
2. G. H. Teppengill, C. C. Counselman, L. P. Rainville, II. Shapiro, Astron. J., **74**, 461, 1969.
3. A. E. E. Rogers, M. E. Ash, C. C. Counselman, I. I. Shapiro, G. H. Pettengill, Radio Science, 5, 465, 1970; Lincoln Laboratory final report, «Radar Studies of Mars», Jan. 15, 1970.
4. R. M. Goldstein, W. G. Melbourne, G. A. Morris, G. S. Downs, D. A. O'Handley, Radio Science, 5, 475, 1970.
5. M. J. S. Belton, D. M. Hunten, Science, **166**, 225, 1969.
6. R. A. Wells, Science, **166**, 862, 1969.
7. K. C. Herr, D. Horn, J. M. McAfee, G. C. Pimentel, Astron. J., 75, 883, 1970.
8. C. A. Barth, C. W. Hord, «Mariner 6 and 7» ultraviolet spectrometer experiment results: topography and polar cap, 1971.
9. M. J. S. Belton, D. M. Hunten, Icarus, 1971.
10. A. Kliore, G. Fjeldbo, B. L. Seidel, S. I. Rasool, Science, **166**, 1393, 1969; A. Kliore, G. Fjeldbo, B. L. Seidel, Summary of «Mariner 6 and 7» radio occultation results on the atmosphere of Mars, COSPAR, 1970.

LETTERS TO NATURE

PHYSICAL SCIENCES

Mars: Are Observed White Clouds composed of H_2O?

MARTIAN clouds have been classified[1] into Type I, which are visible at short optical wavelengths, and become gradually invisible as the wavelength increases; and Type II, which are visible at long wavelengths, and fade into invisibility when the wavelength decreases. The three principal kinds of observed Martian clouds—yellow, white, and blue—can be categorized as Type I, blue; and Type II, yellow and white. This distinction is essential. Yellow and white clouds are classified together because they are visible in the same wavelength range; yellow clouds are dust clouds and will not be described here.

The composition of white and blue clouds is uncertain, although their physical distinction has been evident for some time[2] (Fig. 1). The positive polarization branch for blue clouds between phase angles 0° and 20° implies that they are made up of much smaller particles than white clouds, whose polarization over the same phase angle range is negative. This property explains the separate spectral categorization: smaller particles scatter shorter wavelengths more efficiently than larger particles. I have revised my lists of white cloud occurrences that have been observed on Mars for the past century[3] by measuring the areographic coordinates of the clouds listed in Table IIb of ref. 3 on photographic plates of Mars, and examining the instances of clouds which have been measured polarimetrically.

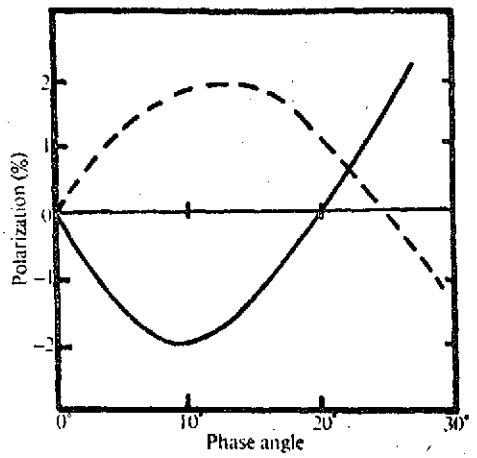

Fig. 1 - - -, Polarization of Martian blue clouds; ——, polarization of Martian white clouds according to Dollfus[2]. Compare the branches between phase angles 0° and 20°.

The value of polarization as a function of phase angle provides a nearly unambiguous means of distinguishing between white, blue, or yellow clouds, thin atmospheric veils, and surface frost deposits. Yellow and white clouds and surface frost have similar appearances on black and white photographic plates, and in the absence of polarization data supplementary information must be used to help distinguish the type of phenomenon. For example, does the phenomenon occur on the limb of the planet; what is the planetocentric location of the occurrence; the season of the Martian year; and the telescopic colour appearance of the phenomenon (if available) at the time the photograph was made, compared with the brightness of the polar cap?

More complete details of Martian clouds and their detection, including the new lists, will be published later.

The revised list of white clouds contains 252 occurrences which are divided as follows: telescopic reports in the literature in which colour distinction and identification as a cloud rely solely on the original observer (1858–1941), 27%; photographic plates in which I made identifications according to the guidelines established previously (1937–1963), 40%; and identification by polarimetric methods (1954–1971), 33%. The percentage categories are listed according to increasing accuracy of identification as white clouds. In those instances where the years of observation overlap the different methods, some clouds were identified by more than one method. This provided a valuable cross-check on the reliability of the less accurate means of identification.

I previously made a comparison[4] between the latitudinal distribution of white cloud occurrences on Mars and the early water vapour data of Schorn *et al.*[5]. In the region of the Martian orbit where their spectra overlapped the cloud distributions, the frequency of white clouds in the northern hemisphere was between three and four times larger than in the southern hemisphere. At the same time, water vapour was more prevalent in the northern hemisphere, indicating that Martian white clouds could be composed of water. But the spectral H_2O data were not very extensive in seasonal coverage so that agreement between white cloud frequencies and the abundance of water vapour could have been fortuitous. Since then, Barker *et al.*[6] have summarized all available H_2O data up to 1969 in the form of a seasonal coverage chart. These data have been revised and extended to 1971 by Tull[7].

I have made a direct comparison of these data with observed white cloud frequencies (Fig. 2) by plotting H_2O abundances and white cloud frequencies against L_s, the planetocentric longitude of the Sun (the heliocentric orbital longitude of Mars, η, and the planetocentric longitude of the Sun are approximately related by $\eta = L_s + 85°$). The 252 clouds were counted in 18° intervals of heliocentric longitude, and the points of the frequency polygon were plotted on the interval mid-points in terms of L_s. On the right ordinate, the relative cloud frequency scale has been adjusted by prior sliding of overlay plots so that the variations in cloud frequency and H_2O vapour can be seen to best advantage.

The top diagram shows the cloud frequencies compared with the original H_2O measurements. The filled circles in the range $280° < L_s < 360°$ are recent observations[7] from the 1971 Mars apparition. Those points enclosed within the dashed-line envelope represent measurements made between October 1971 and January 1972 during the maximum activity of the yellow dust storm which enveloped the planet during this period. These observations reflect only the H_2O vapour above the yellow clouds[7]. Observations of global CO_2 pressures[8] and the Mariner 9 photography[9] during the same period indicate that the tops of the yellow clouds are at an altitude of either 10 km or 40 km depending on whether a single- or multiple-scattering layer model is used.

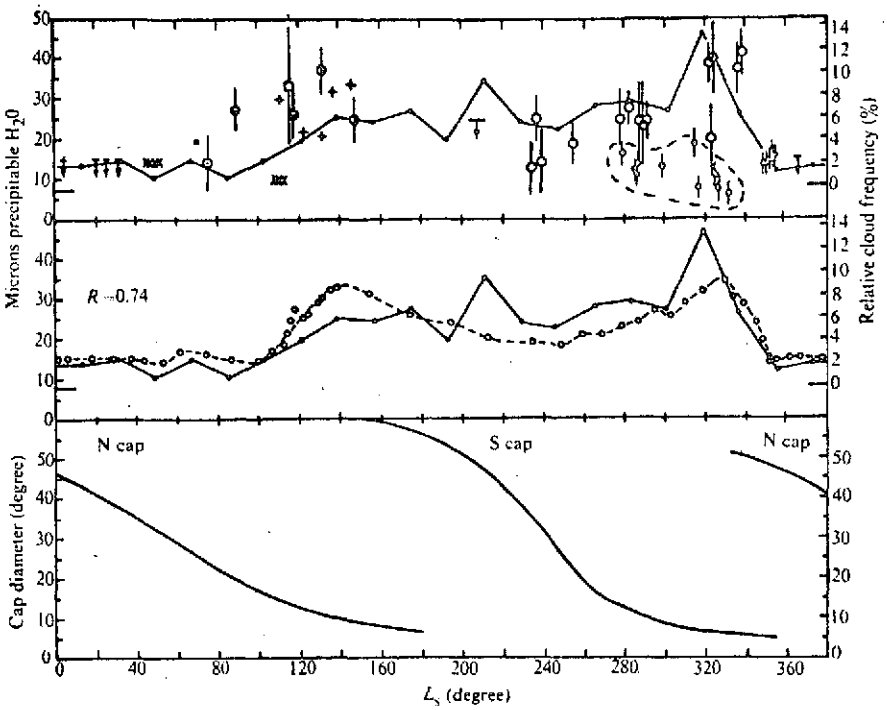

Fig. 2 Global white cloud frequency distribution based on 252 occurrences around the Martian orbit compared with the observed abundance of water vapour as a function of season on Mars. In the upper diagram, vertical arrows point downwards from upper limits, Schorn *et al.*[5]; ×, ◒, Schorn *et al.*[5]; □, Owen[19]; +, ◑, Tull[16]; ○, Kaplan *et al.*[20]; ○, Barker *et al.*[6]; ●, Tull and Barker[7]. In the middle diagram, the cloud frequency (●—●) is compared with a 5-point running average of the H_2O data (○ - - - ○) in the upper diagram, omitting the points enclosed by the dashed envelope. The lower diagram shows the polar caps diminishing with season as determined by Antoniadi[10].

The other five points between about $L_s = 350°$–$360°$ refer to observations made towards the end of February and the beginning of March 1972 after the dust storm had subsided.

The middle diagram shows the distribution of cloud frequencies compared with a five-point running average of the H_2O data points in the upper diagram. The ten points enclosed by the envelope in the top diagram were omitted from this averaging process because of the influence of the dust storm.

Table 1 Rank Correlations and Significance Levels for Figs. 2 and 3

Significance level	Normal z deviate	Spearman's R	No. ranks	s.e.	Calc. z deviate	Null hypothesis rejected
0.200	0.67					
0.100	1.65	0.74	20	0.229	3.23	Yes
0.050	1.96	0.56	7	0.408	1.37	No
0.020	2.33	0.94	6	0.447	2.10	Yes
0.010	2.58					
0.001	3.29					

A peak in cloud frequency of 9.5% at $L_s = 211°$ appears to be out of place. It would have been desirable to have had more H_2O data between $L_s = 150°$–$230°$, but it is clear that the variations in cloud frequencies are correlated with those of the H_2O abundances. For if intervals of cloud frequency are ranked by increasing frequency with the corresponding increases in H_2O abundances, Spearman's rank correlation gives $R = 0.74$.

An exact test for the level of significance of the rank correlation coefficient is laborious since there are 20 ranks; however, if the standard error of R is approximated by $(n-1)^{-1/2} = 0.229$ for the n ranks, then the normal z deviate is $0.74/0.229 = 3.23$. The significance test rejects the null hypothesis because at the 1% level $z = 2.58$ and at the 0.1% level $z = 3.29$ (Table 1). I therefore conclude that the correlation between white cloud frequencies and H_2O abundances is significant.

The bottom diagram of Fig. 2 shows the decreasing size of the Martian north and south polar caps with season[10]. Clearly more H_2O and white clouds occur in the atmosphere when the polar cap size is at a minimum. It is known from observation[11,12] and theory[13,14] that the Martian polar caps are primarily frozen CO_2, although theory admits a two-layer model composed of both frozen CO_2 and H_2O ice. Also, recent measurements[15] from Mariner 9 have indicated the presence of H_2O vapour over the south polar area.

It is interesting to compare H_2O abundances with those of white clouds as a function of latitude on Mars. Tull[16] has published H_2O abundances distributed by latitude and measured on 2 days separated by a month in March and April 1969. During this period, Mars ranged from about η218° to 231° heliocentric longitude. Two 18° intervals contain a statistically significant cloud count corresponding closely to these dates, η216° to 233° and η234° to 251°.

In these intervals 43 clouds occurred and are divided as follows: telescopic reports in classical literature, 12%; identification by photographs, 39%; and identification by polarization, 49%. Clouds were counted in 10° latitude intervals (Fig. 3).

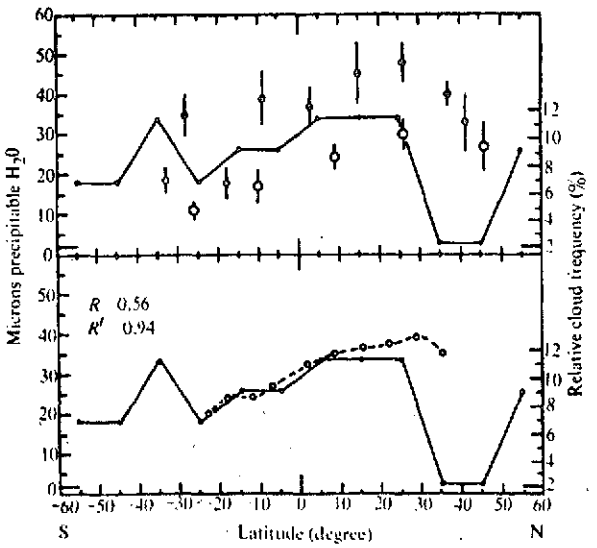

Fig. 3 ●—●, White cloud frequencies distributed by latitude for the portion of the Martian orbit between η216°–251° compared with the H_2O abundances determined by Tull[16]. In the upper diagram, observations for March 27 are denoted by ● and for April 28 by ○. In the lower diagram, the cloud frequency (●—●) is compared with a 5-point running average (○ - - - ○) of the H_2O data in the upper diagram.

The filled circles in the upper diagram are Tull's H_2O abundances for March 27, the open circles for April 28. In the lower diagram a 5-point running average has been applied to the H_2O data. Over the portion of the diagram from about $-30°$ S to about 25° N, the correspondence between the cloud frequencies and H_2O abundances is quite good.

In the lower diagram, there are 7 frequencies between $-25°$ S and 35° N which have matching H_2O data. But for these 7 ranks Spearman's correlation coefficient is only 0.56. For less than 10 ranks a significance test may not be valid; however, line 2 of Table 1 gives the standard error and calculated z deviate. The calculated value, 1.37, does not exceed that expected for the 10% significance level; therefore, the null hypothesis cannot be adequately rejected. On the other hand, if only the 6 points between $\pm 25°$ latitude are ranked with the corresponding water vapour data, $R' = 0.94$. In that case the calculated z deviate, 2.1, exceeds the 5% level and is close to the 2% level; hence, this correlation is probably significant (Table 1).

It is not necessarily the case that observed cloud frequencies will always follow H_2O abundances. In Fig. 2, for example, the trends are averaged over an entire Martian year; in Fig. 3, the trend is a monthly average. Many atmospheric conditions will affect the rates of condensation and/or sublimation and thus cloud formation. In particular, the severe drop in cloud frequency between latitudes 35° and 45° N poses an interesting problem. It suggests that perhaps some atmospheric process is suppressing cloud formation, other factors being equal. But an equally vexing problem is posed by the apparent rise in cloud frequency in the opposite hemisphere at $-35°$ S latitude, if indeed this is real. Over this range of the Martian orbit, the northern hemisphere is experiencing summer, while the southern hemisphere is in winter. This fact may affect the vertical temperature profiles and hence the H_2O condensation rates which could explain the cloud frequency peak in the one hemisphere and the minimum in the other.

Although Martian white cloud frequencies tend to follow the distribution of H_2O both seasonally and latitudinally on the planet, which strongly suggests that most white clouds are formed from water vapour, evidence for the composition of the blue clouds is still lacking.

Polarization data (Fig. 1) indicated that blue clouds are composed of much smaller particles than white clouds. This distinction implies either a different composition for blue clouds or a different physical environment in which they form, or both. The observation by Herr and Pimentel[17] of solid CO_2 crystals above the planetary limb during the flights of Mariners 6 and 7 and the meteorological analysis of this observation by Hess[18] indicate the possibility of two layers of condensation on Mars. Hess[18] pointed out that if CO_2 condensation takes place in the upper atmosphere of Mars, then H_2O condensation at lower levels is almost a certainty. So it is possible therefore that Martian blue clouds are composed of CO_2 ice.

I thank R. G. Tull for an advanced copy of the Martian H_2O observations conducted at MacDonald Observatory and the seasonal coverage chart, and A. Dollfus for permitting examination of the detailed collection of polarization measurements and the photographic plates at the IAU Mars Data Centre, Observatoire de Paris, Meudon. This investigation was supported by a NASA grant.

R. A. WELLS

Space Sciences Laboratory,
University of California,
Berkeley 94720

Received March 21, 1971; revised May 15, 1972.

[1] Wright, W. H., *Lick Obs. Bull XIII*, 389, 50 (1927).
[2] Dollfus, A., thesis, Univ. Paris (1955).
[3] Wells, R. A., *An Analysis of Martian Clouds and Their Topographical Relationships*, ESRO Scientific Note 54 (1966).
[4] Wells, R. A., *Astrophys. J.*, **147**, 1181 (1967).
[5] Schorn, R. A., Spinrad, H., Moore, R. C., Smith, H. J., and Giver, L. P., *Astrophys. J.*, **147**, 743 (1967).
[6] Barker, E. S., Schorn, R. A., Woszczyk, A., Tull, R. G., and Little, S. J., *Science*, **170**, 1308 (1970).
[7] Tull, R. G., and Barker, E. S., *Ground-Based Photoelectric Measures of H_2O on Mars during the Mariner 9 Encounter* (Amer. Astron. Soc., Div. Planet. Sci. Conf., 1972).
[8] Parkinson, T. D., and Hunten, D. M., *Science*, **175**, 323 (1972).
[9] Masursky, H., *et al.*, *Science*, **175**, 294 (1972).
[10] Antoniadi, E. M., *La Planète Mars* (Hermann, Paris, 1930).
[11] Herr, K. C., and Pimentel, G. C., *Science*, **166**, 496 (1969).
[12] Neugebauer, G., *et al.*, *Science*, **166**, 98 (1969).
[13] Leighton, R. B., and Murray, B. C., *Science*, **153**, 136 (1966).
[14] Leovy, C. B., and Mintz, Y., *J. Atmos. Sci.*, **26**, 1167 (1969).
[15] Hanel, R. A., *et al.*, *Science*, **175**, 305 (1972).
[16] Tull, R. G., *Icarus*, **13**, 43 (1970).
[17] Herr, K. C., and Pimental, G. C., *Science*, **167**, 47 (1970).
[18] Hess, S. L., *J. Atmos. Sci.*, **27**, 1117 (1970).
[19] Owen, T., *Science*, **165**, 893 (1969).
[20] Kaplan, L. D., Münch, G., and Spinrad, H., *Astrophys. J.*, **139**, 1 (1964).

11.1

R. A. WELLS

Space Sciences Laboratory,
University of California,
Berkeley, California 94720, USA

Martian, Lunar, and Terrestrial Crusts: A 3-Dimensional Exercise in Comparative Geophysics

Five years ago Runcorn (1967) wrote that '. . . the possibility of convection makes a careful study of planetary surfaces for indications (however different from those of the Earth's surface) of internal activity, volcanic or tectonic, even of the most feeble kind, of great scientific significance.'

Although covering only about 10% of the Martian surface, the photographs returned by Mariners 4, 6, and 7 revealed little in the way of internal crustal activity. Some tectonic evidence in the form of parallel lineaments and polygonal crater walls was all that could be gleaned from these photographs pertaining to internal mechanisms at work on Mars.

However, this situation changed dramatically even with the first few photographs of the surface taken by Mariner 9 after the planet-wide dust storm cleared in mid-January 1972. These photographs revealed indisputable calderas with all of the terrestrial morphology present: rising shields surmounted by lava channels, the primary caldera with smaller subsidiary craters in their floors, stepped benches on the inside of crater walls, and both arcuate and radial fault patterns surrounding each province. Later photos showed widespread lava flows, sinuous lunar-like rilles, large-scale fractures, and massive faulting and slumping. In one case in particular, a rift zone was discovered near the Martian equator extending 5000 km in a nearly east–west direction with widths approaching 100 km. The depth of the main fracture varied from 2 to 7 km along this length. 5000 km on Mars is approximately 80° of longitude, nearly a quarter of the distance around the circumference. Thus, the feature is even more imposing than the East African Rift System.

In a large proportion of photographs, many features were clearly controlled by a tectonic grid pattern indicating orthogonal sub-surface prestressing prior to the eventual surface expression. (See McCauley *et al.* (1972) for photo geology.)

The major geological feature on Mars can be summarized with one word—volcanism. Although this revelation does not necessarily imply that convective processes have operated in the Martian mantle, it nevertheless points to far more crustal activity than had been supposed.

Prior to these later discoveries, the author (Wells, 1969a, b, 1971) put forward the hypothesis of continental drift and sea-floor spreading to account for *presumed* continental-type blocks and basin structures on Mars. This hypothesis gained support

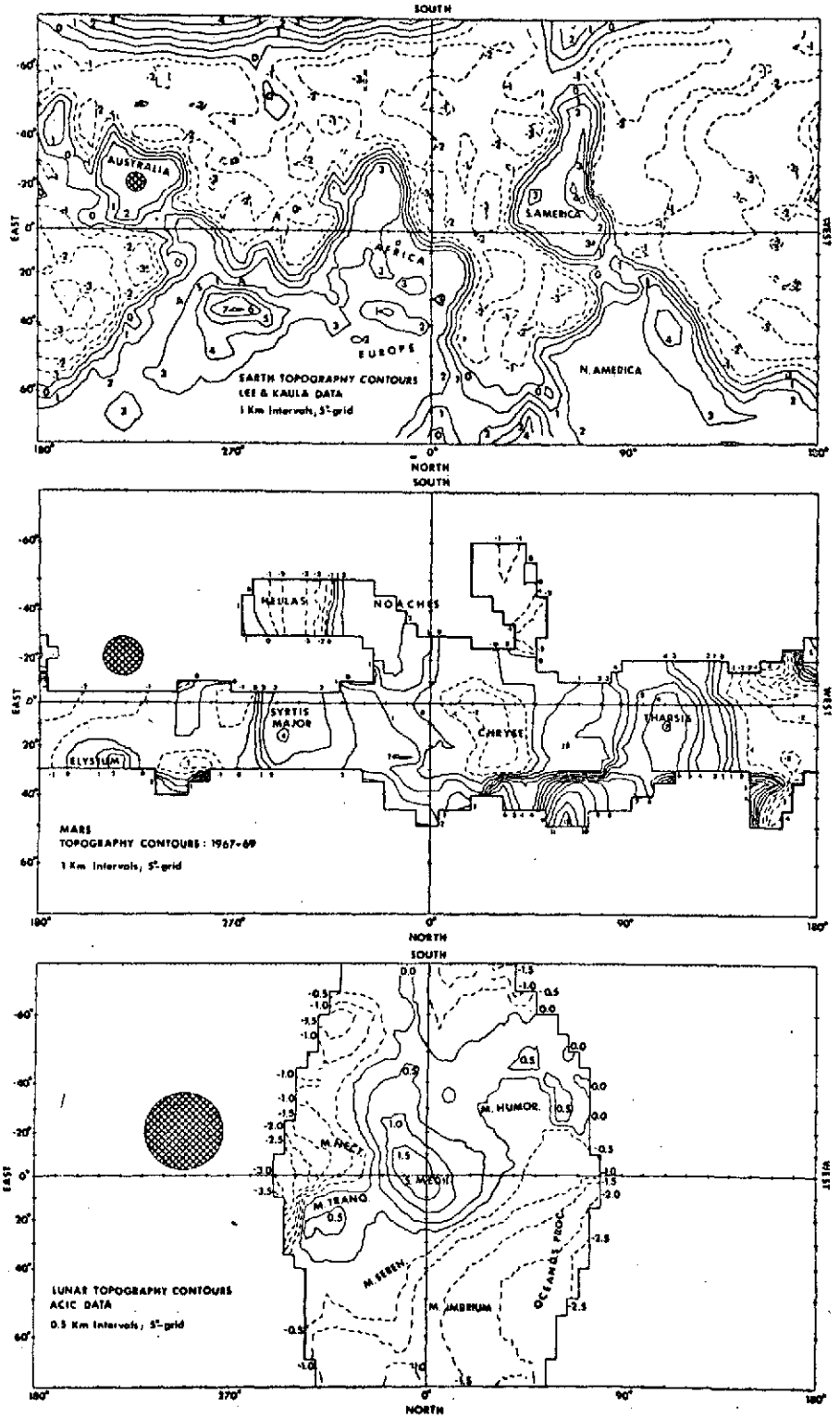
SOUTH
AUSTRALIA
S.AMERICA
AFRICA
EUROPE
N.AMERICA
EARTH TOPOGRAPHY CONTOURS
LEE & KAULA DATA
1 Km Intervals, 5°-grid
EAST
WEST
180°
270°
0°
90°
180°
NORTH
SOUTH
HELLAS
NOACHIS
SYRTIS MAJOR
CHRYSE
THARSIS
ELYSIUM
MARS
TOPOGRAPHY CONTOURS : 1967-69
1 Km Intervals, 5°-grid
NORTH
SOUTH
M. HUMOR.
M. NECT.
M. FRIGO
M. SERENI.
M. IMBRIUM
OCEANUS PROC.
LUNAR TOPOGRAPHY CONTOURS
ACIC DATA
0.5 Km Intervals, 5°-grid
NORTH

FIGURE 1

when actual blocks and basins were eventually mapped (Wells, 1969c, 1971, 1972) on a scale whose areal extent matched the blocks and basins of the Earth. The Martian features were revealed in a contour map (Wells, 1972) prepared from the combination of Earth-based radar ranging data, Earth-based CO_2 pressure measurements over resolved Martian areas, and the Mariner 6 and 7 IRS and UV pressure determinations along limited tracks on the Martian surface.

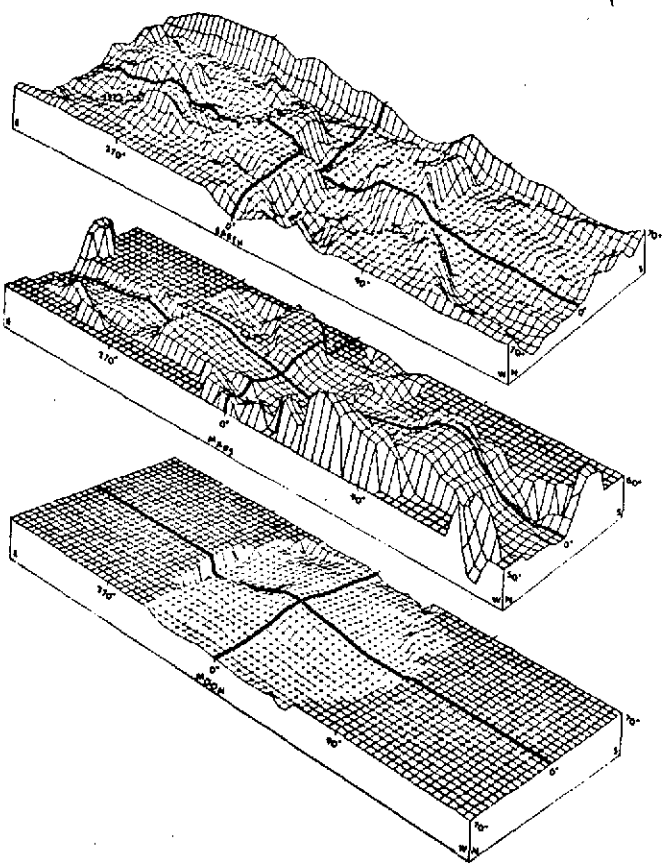

FIGURE 2 Perspective views of the Earth, Mars, and the Moon drawn by computer from the same 5° grid arrays used to construct the contour maps shown in Fig. 1. Views are looking towards the SE from a point inclined 20° to the horizontal. The vertical scale has been exaggerated twice and is the same for each body to permit direct comparisons. However, the blocks seen on Mars at 180°, 20° S; 150°, 45° N; and 245°, 40° N are artifacts produced by the lack of reliable data at the map edges in these areas. For Mars and the Moon, the flat, stippled areas denote unobserved regions and are set at the zero level; hence, slopes bordering their edges are fictitious.

FIGURE 1 Contour maps of the Earth, Mars, and the Moon. The zero level refers to the mean radius of each body. For the Earth, the 1° grid data of Lee & Kaula (1967) were processed onto a 5° grid and each data point smoothed to a resolution of 1000 km so that the scale of the contour map would be the same as for Mars. The lunar contour map was prepared from the A.C.I.C. (Meyer & Ruffin, 1965) selenodetic control measurements in the same manner. The 1000 km resolution is denoted by the cross-hatched circle at the left of each map. The computer contour program is based on linear interpolation between adjacent grid points.

The data from this contour map have been plotted by a computer in the form of a three-dimensional perspective view. Similarly, the total Earth topography (Lee & Kaula, 1967) and the selenodetic altitude measurements of the lunar front-face (Meyer & Ruffin, 1965) were processed by the same equations to the same scale used for the preparation of the Martian contour map.

Figure 1 compares the contour maps of the Earth, Mars, and the Moon prepared in this fashion. South is placed at the top to conform with the Astronomical convention of depicting maps of the Moon and planets. The cross-hatched circle on the left of each contour map represents the resolution (1000 km) of each data point in the 5° grid of values contoured by the computer. This resolution is set by the best available for the Martian contour map. The zero level in each case refers to the mean radius of the body concerned.

Figures 2 and 3 show the comparison of the large-scale features in perspective for the three bodies. Vertical scales are the same for each of the three views to permit

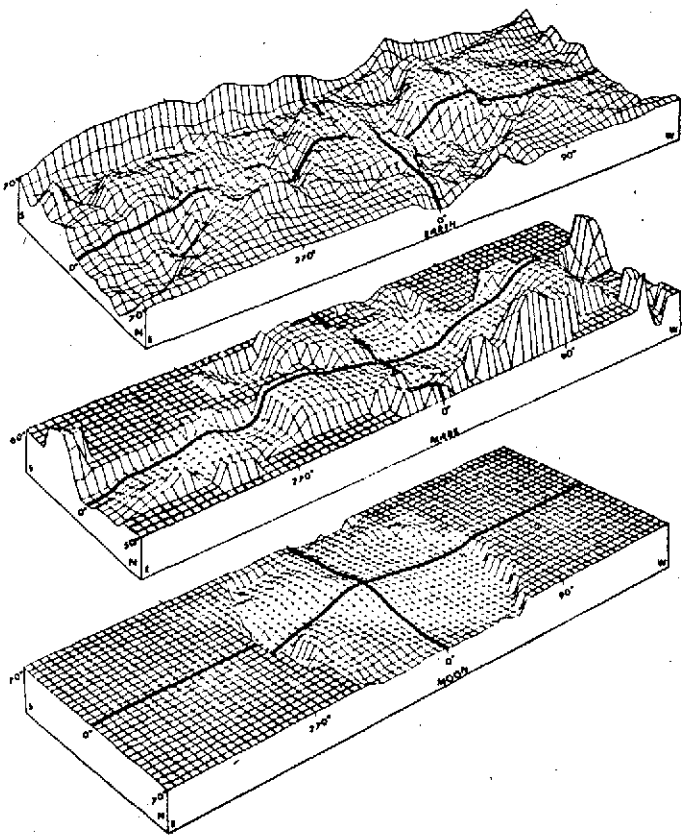

FIGURE 3 Perspective views of Earth, Mars, and the Moon rotated 90° with respect to Fig. 2. The views are looking towards the SW from an elevation angle of 20°.

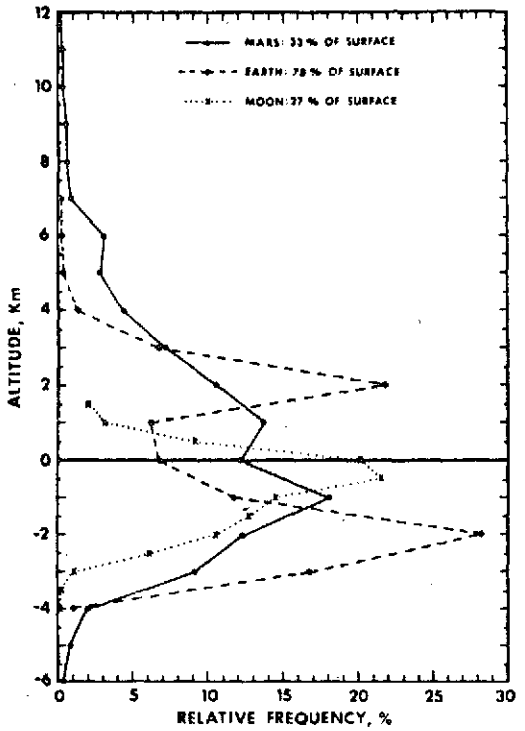

FIGURE 4 A comparison of the hypsometric curves of the Earth, Mars, and the Moon prepared by tracing the contours of Fig. 1 on an equal area projection. The abscissa denotes the areal frequency and the ordinate the altitude of the surface. The fractional areas mapped for each body are listed with the symbol definitions in the inset. Zero altitude refers to the mean radius of the body concerned.

a direct comparison of the sizes of the features seen. Grid intervals are 5° in both latitude and longitude for each case.

It is evident that the blocks and basins on Mars are more nearly comparable with those on the Earth than with those on the lunar crust which reveals only gradual undulations. The range of heights for the Earth is 11 km; for Mars 18 km; and for the Moon 5 km.

Hypsometric analyses of the three contour maps drawn on an equal area projection are given in Fig. 4. An interpretation of the nature of the peaks in areal frequency as a function of altitude in terms of isostatic mechanisms cannot be made without supplementary information regarding the density, temperature, and compositional distributions within the bodies. However, a bi-modal distribution does imply a change in slope from the highest features to the low points of basins; whereas a unimodal distribution signifies a constant slope from the tops of the highest areas to the bottoms of the lowest regions. Thus, Fig. 4 also implies that the Martian crust is, at least geometrically, more like the Earth than the Moon.

The presence of large-scale blocks and basins on Mars, and the recently detected widespread volcanism, extensive faulting and rifting of the Martian crust do not, of course, guarantee a 'continental drift and sea-floor spreading' theory for Mars, which may be even more difficult to firmly establish than it has been in the terrestrial

case; but they at least strongly suggest that Mars has at some time in its history undergone formative processes similar to those of the Earth.

Within the next few years, the study of the Martian crust and the development of a Martian geophysics will undoubtedly provide valuable information of interest to the terrestrial environmental sciences.

A more complete discussion of Martian geophysics, including current spacecraft results integrated with past Earth-based observations, can be found in Wells (1973).

Supported by NASA grant NGR 05–003–431.

References

Lee, W. and Kaula, W. M., 1967. *J. Geophys. Res.*, **72**, 753.

McCauley, J. F., Carr, M. H., Cutts, J. A., Hartmann, W. K., Masursky, H., Milton, D. J., Sharp, R. P., and Wilhelms, D. E., *Icarus*, **17**, 289 (1972).

Meyer, D. L. and Ruffin, B. W. *Icarus*, 4, 513 (1965); A.C.I.C. Tech. paper No. 15, March (1965); A.C.I.C. Report RM-698-1, October (1966).

Runcorn, S. K., 1967. *In:* Mantles of the Earth and Terrestrial Planets, edited by S. K. Runcorn, p. 513. Interscience (Wiley), London.

Wells, R. A., *Geophys. J.R.A.S.*, **17**, 209 (1969a); *Ibid.*, **18**, 109 (1969b); *Science*, **166**, 862 (1969c); *Phys. Earth Planet. Interiors*, **4**, 273 (1971); *Geophys. J.R.A.S.*, **27**, 101 (1972); *Morphology of the Planet Mars*, D. Reidel, Dordrecht, in preparation (1973).

D. REIDEL PUBLISHING COMPANY, INC./BOSTON-U.S.A.

306 DARTMOUTH STREET - BOSTON, MASS. 02116, U.S.A. - TELEPHONE (617) 536-5532 - TELEX 940541

Series	ASTROPHYSICS AND SPACE SCIENCE LIBRARY 43
Title	MORPHOLOGY OF THE PLANET MARS
Author	R. A. Wells (University of California, Berkeley, Calif.)
Other Info.	1974, approx. pp. LC 72-92537 Cloth, approx. Dfl. .- / U.S. $ ISBN 90-277-0150-4

Text

In the past twenty years, published investigations concerning the planet Mars have steadily increased. Through the successes of a number of American and Soviet space probes, knowledge of the Martian surface and atmosphere has been brought into sharper focus than ever before. This text deals with the basic Earth-based research conducted during this period with references to classical problems and integrates these results with those obtained from spacecraft observation.

The following topics are among many discussed: The Chemical Composition and Physical Properties of the Atmosphere presents a summary of spectroscopic investigations; deals with the chief optical influence of the atmosphere which is characterized by Mie suspensions of fine dust particles; and presents statistics of principal cloud occurrences (yellow-dust particles and white H_2O crystals).

The Nature of the Surface discusses the geochemical compositional inferences from visible and near-infrared reflection spectra;

presents the morphology of the polar caps and surface from Mariners 4, 6 and 7 near-encounter photos and a large selection of the most intriguing of the Mariner 9 photos; and shows the classical problem of the so-called "oases and canal" system resolved into low albedo floored craters, low albedo collared volcanic calderas, and chains of large-diameter craters and low albedo terrain alignments.

The Topography and Geophysics of Mars. The topography of the surface is treated at length and contour maps of surface elevations are given with respect to a sphere, the solid-surface triaxial ellipsoid figures, and the dynamic ellipsoid or "areoid". Also discussed are observations of the Martian gravity field calculated from perturbations on the orbits of Mariner 9; the non-hydrostatic figure of Mars which is shown from Mariner 9 occulation measurements to be real and to agree essentially with the Earth-based optically determined flattening of the planet; gravity anomalies and areal frequency distributions of surface elevations which show that Mars possesses blocks and basins similar to the terrestrial continents and ocean basins; and, finally, the relationship between the gravity field and stresses in the crust calculated and related to convextion in the mantle and its implications of possible continental drift on the surface.

Each chapter contains an extensive bibliography. The text is profusely illustrated and contains fold-out charts of the

airbrush renditions of the Mariner 9 photomosaic coverage of the whole planet.

Contents

Preface - Introduction.

Part I: The Atmosphere of Mars. - 1. Extent of the Atmosphere. 2. Chemical Composition of the Atmosphere. 3. Physical Properties of the Atmosphere.

Part II: The Martian Atmosphere in Relation to the Surface. 4. Martian Cloud Systems, Wind Patterns, and Frequency Distributions. 5. The Seasonal Darkening Wave.

Part III: The Surface of Mars. 6. The General Surface Topography. 7. The Existence and Structural Nature of Martian Canals. 8. The Martian Grid System. 9. Mantle Convection and Continental Drift on Mars.

Author Index. - Subject Index. - Back Pocket Fold-Out Mariner 9 Charts.

Audience

Graduate students in physical sciences: astronomy, planetary astronomy, geology, geophysics and meteorology.
